ELSEVIER

Coastal Engineering 46 (2002) 61–87

Coastal Engineering
An International Journal for Coastal, Harbour and Offshore Engineers

www.elsevier.com/locate/coastaleng

Phase lags in oscillatory sheet flow: experiments and bed load modelling

C. Marjolein Dohmen-Janssen *,[1], David F. Kroekenstoel, Wael N. Hassan, Jan S. Ribberink

Department of Civil Engineering, University of Twente, PO Box 217, 7500 AE Enschede, The Netherlands

Received 7 February 2001; received in revised form 14 March 2002; accepted 12 April 2002

Abstract

Sheet flow corresponds to the high velocity regime when small bed ripples are washed out and sand is transported in a thin layer close to the bed. Therefore, it is often assumed that sand transport in oscillatory sheet flow behaves quasi-steady: time-dependent transport rates are assumed to be instantaneously related to the near-bed orbital velocity. However, new experimental results show that even in sheet flow, phase lags between sediment concentration and near-bed velocity can become so large that they lead to a reduction of the net (wave-averaged) transport rate. A phase lag parameter is defined, which shows that phase lags become important for fine sand, high velocities and short wave periods. A semi-unsteady model is developed that includes the effects of phase lags on the net transport rate. New experiments were carried out in a large oscillating water tunnel with three different sands (D_{50} = 0.13, 0.21 and 0.32 mm) for a range of prototype, combined wave–current flow conditions. Measured net transport rates were compared with predictions of a quasi-steady model and the new semi-unsteady model. This comparison indicates that net transport rates are reduced if phase lags become important: the quasi-steady model overestimates the net transport rates and the semi-unsteady model gives better agreement with the data. Time-dependent measurements of velocities and concentrations show that the reduced net transport rates can indeed be explained by phase lag effects, because for tests with smaller net transport rates than predicted by the quasi-steady model, considerable phase lags between velocities and concentrations were observed, even inside the sheet flow layer. Verification of the semi-unsteady model against a larger data set confirms the occurrence of phase lag effects in oscillatory sheet flow. Also for the larger data set the semi-unsteady model yields better agreement with the data than the quasi-steady model.

Keywords: Sediment transport; Sheet flow; Phase lags; Grain size influence; Oscillating water tunnel; Bed load modelling; Quasi-steady transport model; Semi-unsteady transport model

1. Introduction

Accurate predictions of cross-shore transport rates are very important in coastal morphodynamics. Cross-shore transport is mainly caused by the orbital motion of short waves. When waves are high, bed shear stresses due to near-bed orbital velocities become so large (Shields parameter $>0.8-1.0$) that ripples are

* Corresponding author. Tel.: +31-53-489-4209; fax: +31-53-489-5377.

E-mail address: c.m.dohmen-janssen@ctw.utwente.nl (C.M. Dohmen-Janssen).

[1] Formerly of Delft University of Technology.

0378-3839/02/$ - see front matter
PII: S0378-3839(02)00056-X

washed out and the bed becomes flat again (sheet flow). The large shear stresses are associated with high transport rates. Therefore, sheet flow is an important transport regime in cross-shore morphodynamics.

Sheet flow has mainly been studied in laboratory facilities, i.e. oscillating water tunnels, due to difficulties of measuring close to the bed under severe conditions in the field, e.g. Horikawa et al. (1982), Sawamoto and Yamashita (1986), King (1991), Asano (1992), Dibajnia and Watanabe (1992), Ribberink and Al-Salem (1994, 1995), Li and Sawamoto (1995), and Zala Flores and Sleath (1998).

Horikawa et al. (1982) were among the first to measure details of oscillatory sheet flow, like the inception of sheet flow, the thickness of the sheet flow layer, time-dependent concentrations profiles inside the sheet flow layer and resulting sediment transport rates. They found that most of the transport takes places inside the sheet flow layer which has a thickness in the order of 10 mm. These observations were confirmed by the full-scale experiments of Ribberink and Al-Salem (1994). This led to the assumption that sediment transport in oscillatory sheet flow behaves quasi-steady, because if the majority of the sand is transported in the thin sheet flow layer a quick sediment response to the oscillatory flow can be expected. Ribberink and Al-Salem (1995) found indeed that time-dependent concentrations in the sheet flow layer were in phase with the velocity. However, Horikawa et al. (1982) found indications that differences between the accelerating and decelerating phase led to differences in concentration profiles inside the sheet flow layer, indicating that the transport process in the sheet flow layer does not just depend on the velocity (which was the same because of the sinusoidal motion). Moreover, Dibajnia and Watanabe (1992) carried out experiments with short wave periods and found that in many cases the quasi-steady transport model of Madsen and Grant (1976) failed to describe the magnitude and the direction of the net transport rate. They expected phase lags between velocity and concentration to be responsible.

An important parameter in sheet flow is the thickness of the sheet flow layer. This is the layer where sediment concentrations are so high that intergranular forces and sediment-flow interaction forces are important. The sheet flow layer thickness δ_s is closely related to the erosion depth δ_e, which is the distance between the top of the bed at zero velocity (still bed level) and the top of the bed at maximum velocity. For steady flow, Wilson (1987) and Sumer et al. (1996) found a linear relation between the non-dimensional sheet flow layer thickness δ_s/D (with D the grain size of the sediment) and the Shields parameter θ (i.e. the non-dimensional shear stress). Not much is known about the sheet flow layer thickness in oscillatory flow. Asano (1992) found a linear relation between the non-dimensional erosion depth and θ, of the same form as the expressions for δ_s/D of Wilson (1987) and Sumer et al. (1996). Sawamoto and Yamashita found a similar expression for the sheet flow layer thickness.

However, Li and Sawamoto (1995) found that the sheet flow layer thickness cannot solely be described by the Shields parameter, but also depends on the unsteadiness of the flow. Similarly, Zala Flores and Sleath (1998) and Sleath (1999) found that the erosion depth in oscillatory flow depends both on the Shields parameter and on the ratio of inertial to gravity force, which can also be considered as a parameter representing the local flow acceleration (Sleath, 1994):

$$S = \frac{\rho u_a \omega}{(\rho_s - \rho) g} \tag{1}$$

Here ω is the angular frequency ($\omega = 2\pi/T$ with T the wave period). For high values of S ($S > 0.2$) they found that plug flow may occur, i.e. particles start moving as a single block and the thickness of the mobile layer shows a sudden increase. For small values of S ($S < 0.2$) their expression for the erosion depth has the same form as the one by Asano (i.e. a linear relation between the non-dimensional erosion depth δ_c/D and the Shields parameter). Inman et al. (1986) performed measurements in the field and observed that for fine sand ($D_{50} = 0.15$ mm) bursting occurred near the moment of maximum velocity, resulting in a significant increase in the thickness of the sheet flow layer. King (1991) measured similar phenomena for fine sand ($D_{50} = 0.135$ mm) in a large oscillating water tunnel. He expected that bursting was restricted to fine grain sediments. Dohmen-Janssen et al. (2001) also found that in oscillatory flow the sheet flow layer thickness for fine sand ($D_{50} = 0.13$ mm) is significantly

larger than for coarser sand ($D_{50} \geq 0.21$ mm). They derived the following two expressions for the sheet flow layer thickness δ_s:

$$\frac{\delta_s}{D_{50}} = \begin{cases} 35\theta_w & \text{for } D_{50} = 0.13 \text{ mm} \\ 13\theta_w & \text{for } D_{50} \geq 0.21 \text{ mm} \end{cases} \quad (2)$$

Here, θ_w is the maximum Shields parameter, which is calculated based on a wave friction factor according to the formula of Swart (1974) with a bed roughness height k_s equal to the median grain diameter D_{50}. The difference in sheet flow layer thickness between fine sand and the two coarser sands may indicate that for fine sand plug flow occurred. However, the value of the parameter S was never larger than 0.1 and the values for S for fine sand were in the same range (0.03–0.08) as those for the two coarser sands (0.02–0.09).

1.1. Transport models and phase lag effects

To predict sand transport rates in oscillatory flow, different types of models exist. An overview is given by Janssen (1995). Nowadays, many unsteady models have been developed that predict time-dependent profiles of flow velocity and sediment concentration from the mass and momentum balances (e.g. Davies et al., 1997). However, these models do not yet seem to give much better predictions than the more simple formula-based models, which are therefore still often used in engineering practice.

Most formulae that predict transport rates in oscillatory flow are based on the assumption that the sand transport reacts instantaneously to changes in velocity (quasi-steady models, e.g. Bailard, 1981; Ribberink, 1998), which is especially supposed to be valid in sheet flow conditions. The reaction can be considered instantaneous if the phase lag between the sediment concentration or sediment transport and the velocity is small compared to the time scale on which the velocity varies, i.e. the oscillation period T. In that case, asymmetric oscillatory velocities with larger (onshore) velocities during the positive half wave cycle than (offshore) velocities during the negative half wave cycle will lead to positive or onshore *net* sediment transport rates (averaged over the wave cycle), due to the non-linear relation (with a power larger than one) between the velocity and transport rate.

However, Ribberink (1998) expected that even in sheet flow conditions the assumption of quasi-steadiness may not be valid for small wave periods. Such conditions were therefore not included in the derivation of his model. The present paper investigates the validity of the assumption of quasi-steadiness in sheet flow conditions. Both sediment entrainment into the flow and settling of the particles back to the bed takes time. If this response time of the sediment is not small compared to the oscillation period, the concentration will lag significantly behind the velocity and the sediment concentration reaches its maximum value after the moment of maximum velocity. Consequently, the maximum sediment flux will be smaller than in the case of an instantaneous sediment response. Moreover, when the velocity becomes zero (at flow reversal), sediment may still be present in the water column, which can therefore be transported in opposite direction during the following half wave cycle. It may be expected that this effect is stronger during the positive half wave cycle than during the negative half wave cycle, due to the higher velocities and consequently larger entrainment heights during the positive half wave cycle. Phase lags between the near-bed velocity and the sediment concentration may therefore lead to a reduction of the *net* (positive) sand transport rate in asymmetric oscillatory flows. Sheet flow measurements by Dibajnia and Watanabe (1992) and by Ribberink and Chen (1993) indicated that this phenomenon may indeed occur. In their experiments with fine sand in asymmetric oscillatory flows Ribberink and Chen measured *negative* (i.e. 'offshore') net transport rates for conditions with the highest flow velocities. As mentioned above, quasi-steady models will predict increasing positive net transport rates for increasing velocities in asymmetric oscillatory flows.

Phase lags can be characterised by the ratio of the fall time of a sediment particle t_{fall} to the wave period T. The fall time of a sediment particle t_{fall} is equal to δ/w_s, in which δ is the height to which the particle is entrained into the flow and w_s is the settling velocity of that particle:

$$\frac{t_{fall}}{T} = \frac{\delta/w_s}{T} = \frac{\delta}{w_s T} \quad (3)$$

If the fall time of a particle is a considerable proportion of the wave period, phase lags can be expected to become important. The height to which a particle is entrained is expected to increase for increasing flow velocity. This means that phase lag effects can be expected for high velocities, short wave periods and fine sand (small w_s). In sheet flow conditions, sediment is mainly transported close to the bed and thus entrainment heights are small. However, due to high sediment concentrations the settling velocity will be much smaller than the settling velocity of a single particle in still water (hindered settling, e.g. Richardson and Zaki, 1954). Therefore, phase lags may become important, even in sheet flow conditions. In order to take into account phase lag effects without including a full description of the time-dependent velocity and concentration profiles, a semi-unsteady model is developed. If phase lags are small, this semi-unsteady model returns to the quasi-steady model of Ribberink (1998). When phase lags become important, the semi-unsteady model gives reduced *net* transport rates, compared to the quasi-steady model. Both models will be described in more detail in Section 2.

1.2. Experiments

In order to investigate whether phase lags may become important in sheet flow conditions in the field, prototype sediment transport data are required over a range of grain sizes, flow velocities and wave periods. However, data on sand transport in oscillatory sheet flow conditions at prototype scale are scarce. Therefore, new experiments were carried out in the Large Oscillating Water Tunnel (LOWT) of Delft Hydraulics, in which near-bed orbital velocities in combination with a net current can be simulated at full scale.

Net transport rates were measured as well as time-dependent velocities (above the sheet flow layer) and concentrations (above and within the sheet flow layer) for three different uniform sands over a range of flow conditions (varying oscillatory velocities, wave periods and net current velocities). The experimental set-up is presented in Section 3.

1.3. Experimental results and model predictions

Section 4 presents the trend of the net transport rates as predicted by the quasi-steady model of Ribberink (1998) over a range of grain sizes and flow conditions in comparison with the trend observed in the measurements. In Section 5, the experimental results are compared with predictions of the quasi-steady model and of the new semi-unsteady model. Section 6 presents the measured time-dependent concentrations in the sheet flow layer, from which a better insight is obtained concerning the time-dependent process of sediment entrainment and settling of sediment during the wave cycle. Limitations of the semi-unsteady model are discussed in Section 7, which also presents a verification of the model against a much larger data set and the practical relevance of phase lag effects.

2. Sand transport models

2.1. Quasi-steady model of Ribberink (1998)

In this quasi-steady bed load model, all transport in the sheet flow layer is considered as bed load. In oscillatory sheet flow conditions the majority of the sediment is transported inside the sheet flow layer (Horikawa et al., 1982; Ribberink and Al-Salem, 1995), which means that the total transport will only slightly deviate from the bed load component, defined in this way.

The model is basically empirical and based on a large number of oscillatory flow and steady flow data. Data with sand finer than 0.2 mm or wave periods smaller than 3 s were not included in the derivation of the model, because of expected occurrence of phase lag effects and a possible violation of the assumption of quasi-steadiness. It is assumed that the instantaneous sand transport rate is proportional to the difference between the actual time-dependent (skin friction) bed shear stress and the critical bed shear stress. The bed shear stress τ_b is expressed in terms of the (dimensionless) Shields parameter θ:

$$\theta(t) = \frac{\tau_b(t)}{\rho(s-1)gD_{50}} \tag{4}$$

Here ρ is the density of water, s is the relative density ($s = \rho_s/\rho$ with ρ_s the density of sediment), g is the gravity acceleration and D_{50} is the median grain diameter. The sand transport rate q_s is normalised by

the parameter $\sqrt{(s-1)gD_{50}^3}$, which yields the following expression:

$$\frac{q_s(t)}{\sqrt{(s-1)gD_{50}^3}} = m(|\theta(t)| - \theta_{cr})^n \frac{\theta(t)}{|\theta(t)|} \quad (5)$$

In combined wave–current flow a wave–current friction factor f_{cw} (as described in Appendix A) is applied to calculate the bed shear stress: $\tau_b(t) = 1/2\,\rho f_{cw} u^2(t)$. The value of the Shields parameter is included in the expression for the bed roughness height in order to take into account the larger roughness heights in case of sheet flow. The following expressions are used in the formulae for the current friction factor f_c and the wave friction factor f_w, respectively, used to calculate the current-related shear stress, the wave-related shear stress and the combined wave–current shear stress:

$$k_{sc} = \max\{3D_{90};\ D_{50}[1 + 6(\langle|\theta|\rangle - 1)]\}$$

$$k_{sw} = \max\{D_{50};\ D_{50}[1 + 6(\langle|\theta|\rangle - 1)]\} \quad (6)$$

$\langle|\theta|\rangle$ is the time-averaged absolute magnitude of the Shields parameter.

Values of the coefficients m and n are based on many data from laboratory and field experiments with steady flows (flume experiments by Guy et al., 1966; duct experiments by Nnadi and Wilson, 1992; river data by Van den Berg, 1986), oscillatory flows (experiments in oscillating water tunnels by Ribberink and Al-Salem, 1992; King, 1991; Sawamoto and Yamashita, 1986) and oscillatory flows superimposed on a net current (oscillating water tunnel experiments by Ramadan, 1994; Ribberink et al., 1994; Katopodi et al., 1994). Based on these data, Ribberink (1998) found the following values of the coefficients m and n: $m = 11$, $n = 1.65$. With these coefficients, 96% of the 214 predicted net transport rates fell within a factor two of the measured net transport rates.

2.2. New semi-unsteady model

Quasi-steady models are based on the assumption that sand transport reacts instantaneously to changes in velocity. However, there are indications that even in sheet flow phase lags between the velocity and the sediment concentration or sediment transport rate may become so large that they affect the *net* transport rate (e.g. measurements by Dibajnia and Watanabe, 1992; Ribberink and Chen, 1993). Phase lags are a result of the delayed entrainment and delayed settling of sediment particles and can be modelled using an advection–diffusion approach. Davies et al. (1997) present an intercomparison between various time-dependent numerical suspension models, that are based on the advection–diffusion approach. Although these models fail to describe correctly the details of the velocity and sediment concentration profiles inside the sheet flow layer, they yield reasonable predictions of the net transport rates in sheet flow conditions (predictions within a factor 2 of the measurements in almost every case). However, these models require numerical computations that may be too time-consuming in complex morphological models. Therefore, we want to investigate whether a simplified analytical form of the advection–diffusion approach could be used to quantify the phase lag effects on the net transport rates. Thus, our intention is not to describe details of the velocity and concentration profiles in the sheet flow layer correctly, but to characterise the importance of phase lags and correct the net transport rates calculated by a quasi-steady model for the effect of phase lags.

An analytical unsteady suspension approach is used to model the processes of delayed entrainment and delayed settling of sediment particles in the sheet flow layer. Net transport rates are calculated with and without including these phase lag effects and the ratio of these two net transport rates is used as a phase lag correction factor r for the quasi-steady net transport rates:

$$\langle q_s \rangle = r \langle q_s \rangle_{quasi-steady} \quad (7)$$

In this study, the model of Ribberink (1998) is used as the quasi-steady reference model, which is corrected for phase lag effects. However, the correction method could be used for any other quasi-steady transport formula.

Time-dependent sediment transport rates including phase lags ('real' transport rates $q_{s,r}$) and sediment transport rates without phase lags ('quasi-steady' transport rates $q_{s,qs}$) are determined as the product of the free-stream velocity $u_\infty(t)$ (i.e. outside the wave boundary layer) and the integral of the time-dependent 'real' concentration profile $c_r(z,t)$ (with phase lags) or

the time-dependent 'quasi-steady' concentration profile $c_{qs}(z,t)$ (without phase lags):

$$q_{s,qs}(t) = u_\infty(t) \int_0^{z_\infty} c_{qs}(z,t)\ \mathrm{d}z$$

$$q_{s,r}(t) = u_\infty(t) \int_0^{z_\infty} c_r(z,t)\ \mathrm{d}z \tag{8}$$

Here, z_∞ is a level far away from the bed where the concentrations become negligibly small, and $z=0$ is the level of the still bed. It must be mentioned that the flow velocity is not constant over the wave boundary layer but changes in magnitude and phase. However, it is assumed that this calculation method is valid since we are not interested in the exact description of the velocity profiles or the sediment transport rate calculated by this unsteady suspension approach. We just use it to characterise the reduction in sediment transport rate due to phase lags (delayed sediment entrainment and settling). The actual magnitude of the net transport rates is determined by the prediction of the quasi-steady model of Ribberink and a correction factor based on this unsteady suspension approach.

Time-dependent sediment concentrations during the wave cycle $c(z,t)$ are described with the one-dimensional advection–diffusion equation that can be derived from a mass conservation consideration:

$$\frac{\partial c}{\partial t} = \frac{\partial}{\partial z}\left[w_s c + \varepsilon_s \frac{\partial c}{\partial z}\right] \tag{9}$$

Nielsen (1979) showed that for a periodic time-dependent flow, this equation can be solved analytically by assuming a constant sediment mixing coefficient ε_s. The quasi-steady concentration profiles $c_{qs}(z,t)$ can be obtained from Eq. (9) by setting $\partial c/\partial t = 0$. This represents a situation in which the concentration profile adjusts itself immediately to the varying flow conditions during the wave cycle, which means that phase lags are neglected. The real concentration profiles, $c_r(z,t)$, that include phase lags, result from the full solution of Eq. (9).

A simple power-function is applied for the necessary reference concentration (boundary condition), in which the concentration at the bottom is related to a power b of the free-stream velocity $u_\infty(t)$. A power $b=2$ is selected, based on earlier experimental observations (Ribberink and Al-Salem, 1994), which showed that in oscillatory sheet flow the transport rate ($q_s \sim cu$) is approximately proportional to the cube of the free-stream velocity (u^3). The solutions are described in more detail in Appendix B.

The phase lag correction factor r is now calculated as the ratio of the net real and quasi-steady transport rates, $\langle q_{s,r}\rangle$ and $\langle q_{s,qs}\rangle$. Using Eq. (8), it follows that:

$$r = \frac{\langle q_{s,qs}\rangle}{\langle q_{s,r}\rangle} = \frac{\frac{1}{T}\int_0^T \left(u_\infty(t)\int_0^{z_\infty} c_{qs}(z,t)\mathrm{d}z\right)\mathrm{d}t}{\frac{1}{T}\int_0^T \left(u_\infty(t)\int_0^{z_\infty} c_r(z,t)\ \mathrm{d}z\right)\mathrm{d}t} \tag{10}$$

In Appendix B, the derivation of r is presented for the case of a second-order oscillatory flow, with a velocity given by: $u(t)=u_0+u_1\cos(\omega t)+u_2\cos(2\omega t)$, with ω the angular frequency of the wave. The present study focuses on situations with a sinusoidal oscillatory flow ($u_2=0$) with velocity amplitude u_a ($=u_1$), superimposed on a mean current with velocity u_m ($=u_0$). In that case the following expression for r is obtained (see Appendix B):

$$r = \frac{\left(\frac{u_m}{u_a}\right)^2 + \frac{1}{2} + F_1(p)}{\left(\frac{u_m}{u_a}\right)^2 + \frac{3}{2}} \tag{11}$$

with: $p=\varepsilon_s\omega/{w_s}^2$.This shows that the phase lag reduction factor r only depends on the ratio of u_m over u_a and on an analytical function F_1 of the parameter p.

- The ratio of u_m over u_a represents the importance of the net current velocity compared to the oscillatory velocity.
- The ratio of sediment mixing coefficient to settling velocity ε_s/w_s in the parameter p can be considered as a characteristic height δ to which particles are entrained. As the ratio δ/w_s is equal to the fall time of a particle t_{fall} and $\omega=2\pi/T$, it follows that the parameter p is proportional to the ratio of the fall time of a particle and the wave period and therefore characterises phase lag effects (see also Section 1). The parameter p is thus called the phase lag parameter and can be written as:

$$p = \frac{\varepsilon_s\omega}{w_s^2} = \frac{\delta\omega}{w_s} = 2\pi\frac{t_{fall}}{T} \tag{12}$$

In order to show the behaviour of the semi-unsteady model, Fig. 1 presents the phase lag reduction factor r as a function of the phase lag parameter p for different values of u_m/u_a. The figure shows that for small values of p (small phase lags) the value of r is equal to 1. This means that for these cases the new semi-unsteady model predicts the same net transport rates as the quasi-steady model of Ribberink (1998). For increasing values of p, corresponding to increasing phase lags, the value of r decreases, which means that for these cases the new semi-unsteady model predicts smaller net transport rates than the quasi-steady model. The net transport rates are thus reduced if phase lags become important, as explained in Section 1.

For an infinitely large value of u_m/u_a, i.e. for purely steady flow, the reduction factor is always equal to 1. This can be explained by the fact that, by definition, no phase lag effects can occur in steady flow, because the velocity does not vary over time. The larger the oscillatory flow compared to the net current (more wave-dominated conditions), the stronger the phase lag effects become.

It is not immediately clear what value should be used for the height δ to which particles are entrained. In the present study, it is assumed that in sheet flow conditions this height δ is closely related to the sheet flow layer thickness δ_s, because most of the sand is transported inside the sheet flow layer. Here, we use our own expression to calculate sheet flow layer thickness in oscillatory flow (Dohmen-Janssen et al., 2001; Section 1), which is based on data from the same experiments as presented in this paper. By using this expression, possible differences between measured net transport rates and predictions of the new semi-unsteady model due to incorrect predictions of the sheet flow layer thickness are excluded and the verification can be focused on how phase lag effects are modelled.

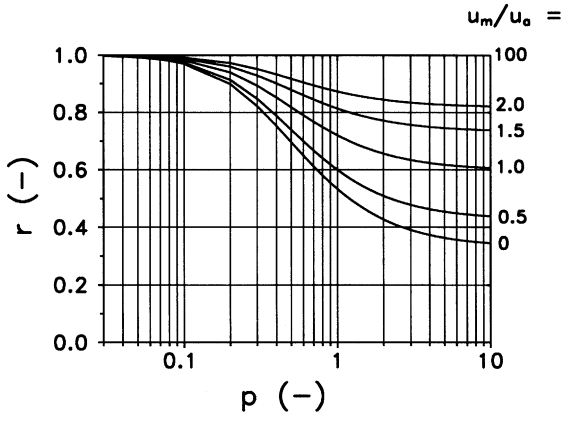

Fig. 1. Calculated values of phase lag correction factor r as a function of phase lag parameter p for different ratios of net current velocity to sinusoidal oscillatory velocity amplitude (u_m/u_a).

An expression for the phase lag parameter as a function of sheet flow layer thickness can be found by substituting Eq. (2) for δ in Eq. (12) and including a calibration coefficient α:

$$p = \alpha \frac{\delta_s \omega}{w_s} = \begin{cases} \dfrac{35\alpha\theta_w D_{50}\omega}{w_s} & \text{for } D_{50} = 0.13 \text{ mm} \\ \dfrac{13\alpha\theta_w D_{50}\omega}{w_s} & \text{for } D_{50} \geq 0.21 \text{ mm} \end{cases} \quad (13)$$

The calibration coefficient α represents the fact that the parameter p is not necessarily exactly equal to $\delta_s\omega/w_s$. This has several reasons. The two most important are:

1. The fact that the characteristic entrainment height δ is not necessarily exactly equal to the sheet flow layer thickness δ_s,
2. The difference between the settling velocity of sediment in the sheet flow layer (with high sediment concentrations) and the fall velocity of a single particle in still water.

Although the latter may be important, there are two reasons why we did not include hindered settling explicitly, but incorporated it in the calibration coefficient α. Firstly, the main aim of the phase lag parameter is to characterise for which conditions phase lag effects become important. Phase lags are especially expected for fine sand, corresponding to a small settling velocity. Sediment concentrations in the sheet flow are approximately the same for different sands, only the thickness of the sheet flow layer varies (Dohmen-Janssen et al., 2001). This means that the relative difference in settling velocity between different sands will be the same whether or not hindered settling is included and that the phase lag parameter can still be used to distinguish whether phase lags are

important or not, even though the actual value of the settling velocity (and thus the phase lag parameter) may be different. Secondly, it can be expected that the eddy viscosity will be reduced due to the large negative concentration gradient over the sheet flow layer which leads to flow stratification and thus to damping of turbulence (e.g. Dohmen-Janssen et al., 2001). Eq. (12) shows that the phase lag parameter depends both on w_s and on the eddy viscosity ε_s. The possible increase in phase lag parameter p due to the effect of hindered settling may be (partly) compensated (or overcome) by a decrease in p due to the reduction in eddy viscosity. This process is neither included explicitly in the phase lag parameter.

3. Experimental set-up

3.1. Large Oscillating Water Tunnel (LOWT)

The new experiments were carried out in the Large Oscillating Water Tunnel (LOWT) of Delft Hydraulics. The LOWT is a U-shaped tube in which near-bed horizontal orbital motions can be simulated at full scale (velocity amplitudes: 0.6–1.8 m/s, wave periods: 2–16 s). A piston in one of the vertical cylindrical risers generates a horizontal oscillatory flow in the test section. The other riser is open to atmosphere. The test section (length: 12 m, width: 0.3 m) can be filled with a 0.3-m-thick sand bed, leaving 0.80 m for the flow. Underneath the cylindrical risers two sand traps are constructed, to collect the sand that is eroded from the test section. Fig. 2 shows the outline of the LOWT.

A recirculation system allows the generation of a net current (velocities of 0–0.5 m/s) in addition to the oscillatory flow. Within the recirculation system a third sand trap is constructed, consisting of a 12-m-long pipe with a diameter of 1.2 m, in order to collect the sand that is transported by the net current and passes the sand trap underneath the riser.

3.2. Test conditions and measured parameters

As mentioned in Section 2, the occurrence of phase lags is expected to depend on the flow velocity, the wave period and the grain size of the sediment. Therefore, experiments were carried out over a range of hydraulic conditions for three different sands. Along the Dutch North Sea coast, sand with a median grain diameter of 0.2 mm is very common. The three sands used in the present experiments were all nar-

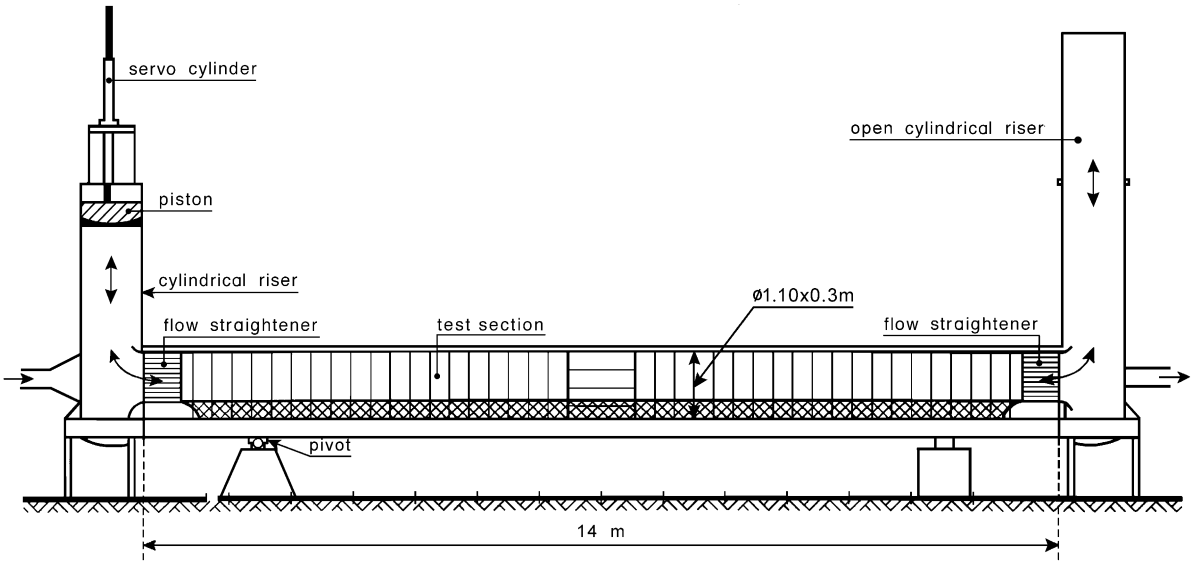

Fig. 2. Outline of the Large Oscillating Water Tunnel of Delft Hydraulics.

row-distributed sands with median grain size equal to $D_{50}=0.13$ mm ('fine sand'), $D_{50}=0.21$ mm ('medium sand') and $D_{50}=0.32$ mm ('coarse sand'). The characteristics of the sands are presented in Table 1. Fig. 3 shows the grain size distributions.

All hydraulic conditions consisted of sinusoidal oscillatory flows with different wave periods and different velocity amplitudes in combination with different net currents. During all conditions, the bed was flat and sheet flow was the dominant transport regime. The test conditions are presented in Table 2. This table presents the actual velocities, as measured at 0.1 m above the sand bed. Two conditions from earlier experiments are included, i.e. E2 and E4 (Katopodi et al., 1994). Table 2 also presents calculated values of the maximum Shields parameters θ_w and θ_{cw}. The latter is based on the measured maximum velocity (u_a+u_m) and a combined wave–current friction factor f_{cw}, as described in Appendix A. Finally, Table 2 presents values of u_m/u_a and calculated values of the phase lag parameter p (Eq. (13), using a value of the calibration coefficient $\alpha=1$, see Section 5). Values of u_m/u_a vary between 0.15 and 0.90, showing that the conditions are mainly wave-dominated. The phase lag parameter p varies between 0.02 and 1.2, indicating that phase lags may become important for some of the tests.

For most conditions, net transport rates were measured. In addition, time-dependent velocities and concentrations at different elevations close to the bed were measured for a few selected conditions (printed bold in Table 2).

3.3. Measuring techniques

Net transport rates were measured using a mass conservation technique, which requires for each test a measurement of the change of sand volume along the test section and of the amount of sand collected in each sand trap. In addition, the run time must be known.

The volume change along the test section was determined by measuring the bed level before and after the test, using a bed level profiling system, developed by Delft Hydraulics (see below). The

Table 1
Characteristics of the three sands used in the present study

	D_{10} (mm)	D_{50} (mm)	D_{90} (mm)	σ_g	w_s (mm/s)
Fine sand	0.10	0.13	0.18	1.30	11.4
Medium sand	0.15	0.21	0.32	1.29	26.0
Coarse sand	0.22	0.32	0.46	1.33	42.9

σ_g = geometric standard deviation = $1/2((D_{50}/D_{16})+(D_{84}/D_{50}))$.

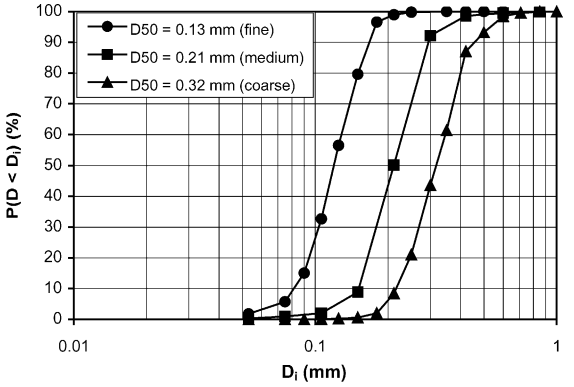

Fig. 3. Grain size distribution of the three sands used in the experiments.

Table 2
Test conditions

Condition	D_{50} (mm)	T (s)	u_a (m/s)	u_m (m/s)	θ_w	θ_{cw}	u_m/u_a	p
H2	0.13	7.2	0.68	0.23	0.74	1.14	0.36	0.26
H3	0.13	7.2	0.93	0.24	1.30	1.85	0.26	0.45
H4	0.13	7.2	1.09	0.25	1.74	2.39	0.23	0.61
H5	0.13	7.2	1.30	0.24	2.40	3.12	0.19	0.84
H6 (D1)	**0.13**	**7.2**	**1.47**	**0.24**	**3.01**	**3.81**	**0.17**	**1.05**
H7	0.13	7.2	0.49	0.42	0.41	1.05	0.90	0.14
H8	0.13	7.2	0.67	0.43	0.72	1.53	0.64	0.25
H9	**0.13**	**7.2**	**0.94**	**0.43**	**1.33**	**2.38**	**0.47**	**0.46**
H24	0.13	4.0	0.68	0.24	0.83	1.29	0.36	0.52
H44 (T1)	**0.13**	**4.0**	**1.06**	**0.25**	**1.84**	**2.52**	**0.23**	**1.15**
H212	0.13	12.0	0.68	0.23	0.67	1.06	0.36	0.14
J1	0.21	7.2	1.06	0.24	1.12	1.53	0.23	0.10
J2	0.21	7.2	1.28	0.25	1.57	2.08	0.19	0.14
E2 (D2)	**0.21**	**7.2**	**1.47**	**0.23**	**2.02**	**2.54**	**0.17**	**0.19**
J3	0.21	7.2	0.46	0.41	0.25	0.66	0.90	0.02
J4	0.21	7.2	0.65	0.41	0.46	0.98	0.64	0.04
E4	**0.21**	**7.2**	**0.95**	**0.44**	**0.92**	**1.65**	**0.47**	**0.08**
J5	0.21	4.0	1.04	0.24	1.22	1.65	0.23	0.20
J6	0.21	12.0	1.09	0.23	1.07	1.45	0.23	0.06
I1 (D3)	**0.32**	**7.2**	**1.47**	**0.26**	**1.44**	**1.86**	**0.17**	**0.12**
I2	0.32	7.2	1.70	0.25	1.87	2.34	0.15	0.16
I3	0.32	7.2	0.65	0.42	0.33	0.71	0.64	0.03
I4	0.32	7.2	0.92	0.42	0.62	1.11	0.47	0.05
I5	0.32	7.2	1.50	0.45	1.49	2.26	0.30	0.13

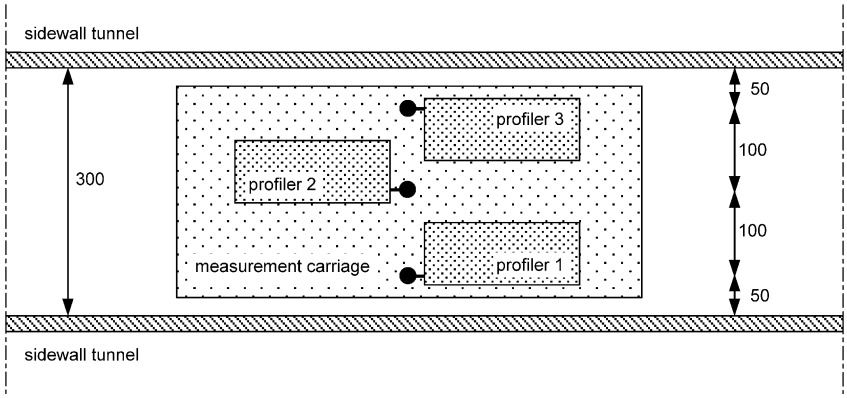

Fig. 4. Schematic diagram of the bed profilers on the measurement carriage.

change of sand volume along the test section is equal to the measured volume change, multiplied by $(1-\varepsilon_0)$, with ε_0 the porosity. The amount of sand in each trap was determined by weighing under water. Run time was determined using a stopwatch.

Net sand transport rates along the tunnel can be calculated by integration from the left- and from the right-hand side boundary of the test section using the sand trap information as boundary condition. This yields two estimates of the net sand transport rate in the middle of the test section:

$$\langle q_{sl}\rangle = \frac{-\Delta V_{l,ip}(1-\varepsilon_0) - \dfrac{G_l}{\rho_s}}{\Delta t W} \tag{14}$$

$$\langle q_{sr}\rangle = \frac{-\Delta V_{r,ip}(1-\varepsilon_0) + \dfrac{G_r}{\rho_s}}{\Delta t W} \tag{15}$$

$\langle q_{sl}\rangle$, $\langle q_{sr}\rangle$ = net sand transport rate in the middle of the tunnel, calculated from the left-/right-hand side (m^3/s m); $\Delta V_{l,ip}$, $\Delta V_{r,ip}$ = volume change of the sand bed (including pores) in the left-/right-hand side of the test section (m^3); ε_0 = porosity of the sand bed in the test section; G_l, G_r = dry mass of sand in the sand trap on the left-/right-hand side (kg); ρ_s = density of the sand (kg/m^3); Δt = run time of the test (s); W = width of the tunnel (m). The bed level profiling system used in the present experiments replaced the hand measurement as used by Ribberink and Al-Salem (1994) and others. The system consists of three bed profilers positioned on a measuring carriage which can be drawn along the test section and a shaft encoder and position counter to determine the horizontal position of the profilers. Fig. 4 presents a schematic diagram of the profilers on the measurement carriage. The bed level profiling system is shown schematically in Fig. 5.

The bed profilers are based on conductivity measurements and are organised such that the conductivity in the sampling volume is kept constant. This means that the probe tip remains at a constant distance from the sand bed. The vertical displacement of the profilers is recorded as a function of the distance along

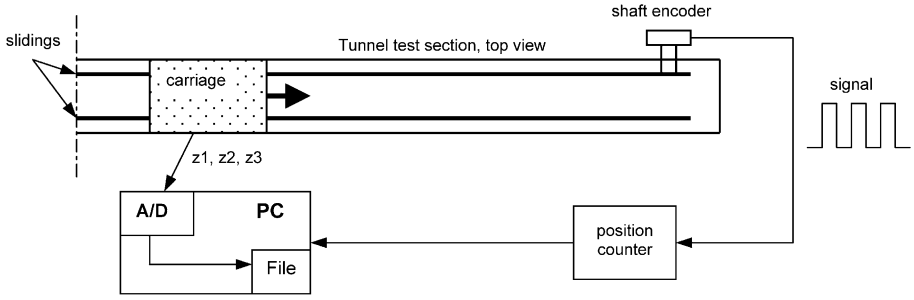

Fig. 5. Schematic diagram of the bed level profiling system.

the test section. The accuracy of the profilers is estimated to be about ± 0.4 mm. A horizontal dummy bottom at the upstream end of the tunnel was used as a reference level.

A 2D-forward scatter Laser-Doppler Anemometer (LDA), developed by Delft Hydraulics (see e.g. Klopman, 1994), was used to measure horizontal and vertical components of flow velocity, without disturbing the flow. The LDA has a small sampling volume, with a height and width (in flow direction) of 0.22 mm. The width in cross-direction is 6.5 mm. With the LDA it is not possible to measure very close to the bed, due to blockage of the laser beams by sediment particles.

A Conductivity Concentration Meter (CCM), developed by Delft Hydraulics, was used to measure concentrations in the sheet flow layer and inside the sand bed. This instrument measures high sand concentrations (≈ 100–1600 g/l) with a four point electro-resistance method (see e.g. Ribberink and Al-Salem, 1995). The measured signal is proportional to the electro-resistance of the sand–water mixture in a small sensing volume directly above the electrodes. The distance between the electrodes is 0.6 mm and the electrodes have a thickness of 0.3 mm. Fig. 6 shows a detailed plot of the CCM probe. The horizontal length of the sensing volume is approximately 2 mm. The height of the sensing volume (above the ends of the electrodes) is approximately 1 mm. The CCM was installed into the tunnel from below, through the tunnel bottom, in order to minimise flow disturbance (see Fig. 7).

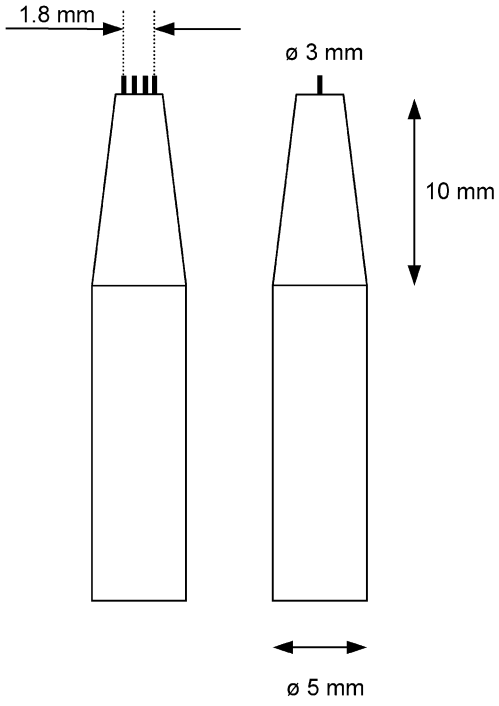

Fig. 6. Schematic diagram of CCM probe.

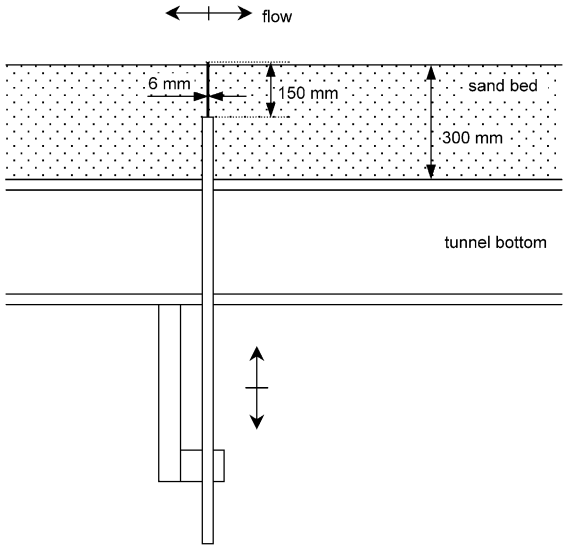

Fig. 7. Configuration of CCM in the tunnel.

In addition, time-dependent suspended sediment concentrations were measured using an Optical Concentration meter (OpCon). Time-averaged concentration profiles of suspended sediment were measured using a Transverse Suction System. Velocities closer to the bed (but above the sheet flow layer) were measured using a 3D-Acoustic Doppler Velocimeter (ADV). These measurements are not included in this paper, but can be found in Dohmen-Janssen (1999).

4. Measured net transport rates and comparison with a quasi-steady model

For each condition, several tests were carried out. Table 3 presents the average net transport rate (i.e. averaged over all tests for each condition) per

Table 3
Measured net transport rates

Condition	$\langle q_{s,avg}\rangle$ (10^{-6} m^2/s)	σ (%)	N	$\langle q_{s,corr}\rangle$ (10^{-6} m^2/s)
H2	15.7	7.0	5	18.8
H3	29.1	9.6	4	34.9
H4	33.3	12.3	3	40.0
H5	43.1	11.4	3	51.7
H6	54.6	22.0	9	65.5
H7	13.0	13.1	3	15.6
H8	39.5	6.1	3	47.4
H9	71.4	7.8	4	85.7
H24	10.2	2.9	3	12.8
H44	8.1	104	5	9.0
H212	16.0	0.9	4	19.9
J1	39.3	6.9	3	46.3
J2	63.6	3.1	3	74.4
E2	*96.4*	*7.5*	*4*	*111.8*
J3	7.2	3.6	3	9.0
J4	20.6	2.1	3	25.3
E4	*71.0*	*9.3*	*4*	*84.4*
J5	24.7	1.3	3	29.2
J6	41.7	1.7	4	49.2
I1	79.7	3.0	4	94.0
I2	129.1	3.4	3	152.3
I3	19.2	9.0	3	23.6
I4	44.1	5.3	3	53.3
I5	162.8	1.5	3	193.7

unit width $\langle q_{s,avg}\rangle$ and the relative standard deviation σ:

$$\sigma = \sqrt{\frac{1}{N}\sum_{i=1}^{N}\left(\frac{\langle q_{s,i}\rangle - \langle q_{s,avg}\rangle}{\langle q_{s,avg}\rangle}\right)^2} \tag{16}$$

N is the number of tests per condition, which is also given in Table 3. Measured net sand transport rates represent the width-averaged value. Due to boundary layers along the side walls of the tunnel, velocities are not constant over the width of the tunnel. In order to be able to relate the measured (width-averaged) net transport rates to the velocities measured in the centreline of the tunnel, the measured net transport rates are corrected. The corrected net transport rates $\langle q_{s,corr}\rangle$ are based on a measured net current velocity distribution over the width of the tunnel and the assumption that the net transport rate is proportional to the third power velocity moment $\langle u^3\rangle$ (see Dohmen-Janssen, 1999). In the further analysis, the corrected values of the net transport rate are used.

As was shown in Section 2, the quasi-steadiness of the transport process and the occurrence of phase lag effects is strongly determined by the parameter p, which in turn is a function of the flow velocity, the grain size (or settling velocity) and the wave period. Therefore, the trend in the measured net transport rates is first analysed as a function of these individual parameters. This is compared with the trend in the net transport rates as predicted by the quasi-steady model of Ribberink (1998).

- Fig. 8 shows $\langle q_s\rangle$ as a function of oscillatory velocity amplitude (u_a) for different grain sizes.
- Fig. 9 shows $\langle q_s\rangle$ as a function of grain size (D_{50}) for different oscillatory velocity amplitudes. The wave period in Figs. 8 and 9 is equal to 7.2 s.
- Fig. 10 shows $\langle q_s\rangle$ as a function of wave period (T) for different combinations of oscillatory velocity amplitude and grain size.

In all cases, the flow velocity consists of a sinusoidal oscillatory component superimposed on a net current with a constant velocity of $u_m = 0.25$ m/s. The left-hand-side panels show the predictions by the quasi-steady model of Ribberink (1998) and the right-hand-side panels show the measurements.

Figs. 8 and 9 show that for small oscillatory velocities (i.e. $u_a \leq 1.1$ m/s, corresponding to values of the maximum Shields parameter $\theta_w < 1$), the quasi-steady model of Ribberink predicts almost the same net transport rates for different grain sizes. When the velocity increases so far that the Shields parameter becomes larger than 1, the predicted net transport rates increase strongly, with increasing net transport rates for decreasing grain size.

However, for the fine sand, the measurements do not show such strong increase in $\langle q_s\rangle$ in the high velocity regime (Fig. 8). As the grain size decreases from 0.21 to 0.13 mm, the measurements show a marked decrease rather than an increase in $\langle q_s\rangle$, contrary to the prediction by the quasi-steady model (Fig. 9).

Fig. 10 shows that the model of Ribberink predicts increasing net transport rates for decreasing wave periods. But, for relatively long wave periods ($T \geq 5$ s) the influence of the wave period on the predicted

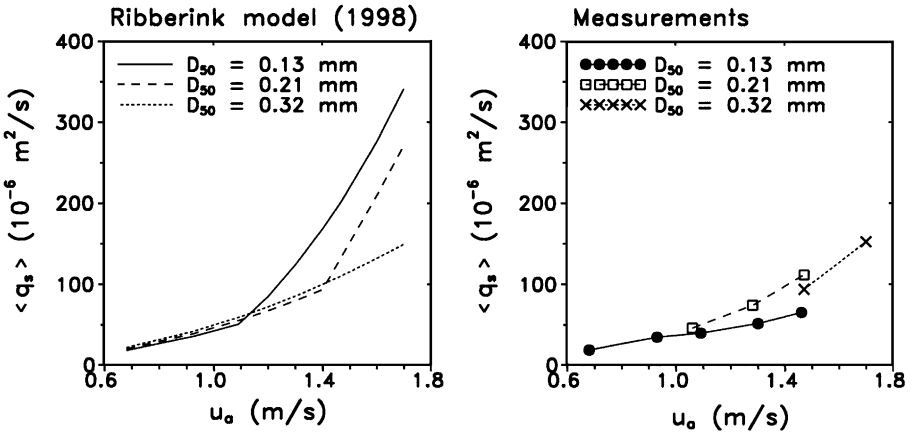

Fig. 8. Net transport rates against oscillatory velocity amplitude for $T=7.2$ s and three different grain sizes; left-hand-side panel: predictions by the quasi-steady model of Ribberink (1998), right-hand-side panel: measurements.

net transport rates is small. The increasing transport rates could be explained by the increasing shear stress due to the increasing relative roughness height. When the value of the maximum Shields parameter becomes larger than 1 (0.13 mm sand, $u_a=1.1$ m/s, $T<5$ s), the predicted increase in net transport rate with decreasing wave period becomes very strong.

The measurements, on the other hand, show the opposite behaviour, i.e. decreasing transport rates for decreasing wave periods when $T<7$ s. For conditions with relatively long wave periods ($T\geq 7$ s) the influence of the wave period on the net transport rates is small, in agreement with the trend of the quasi-steady model.

Figs. 8–10 show that for certain parameter ranges the trend of the net transport rates is predicted reasonably well by the quasi-steady model. However, in other ranges (fine sand, high velocities, short wave periods), clear differences are observed between the predicted and the measured trend. These cases all correspond to relatively high values of the phase lag parameter p. According to the presented semi-

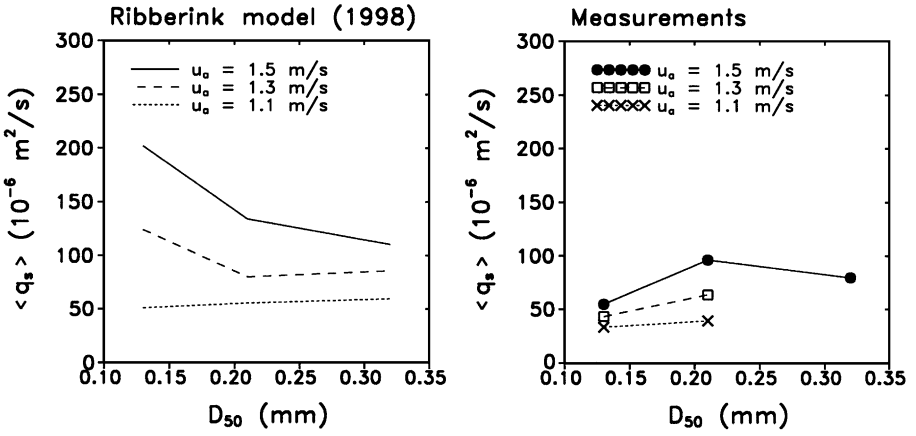

Fig. 9. Net transport rates against grain size for $T=7.2$ s and different oscillatory velocity amplitudes; left-hand-side panel: predictions by the quasi-steady model of Ribberink (1998), right-hand-side panel: measurements.

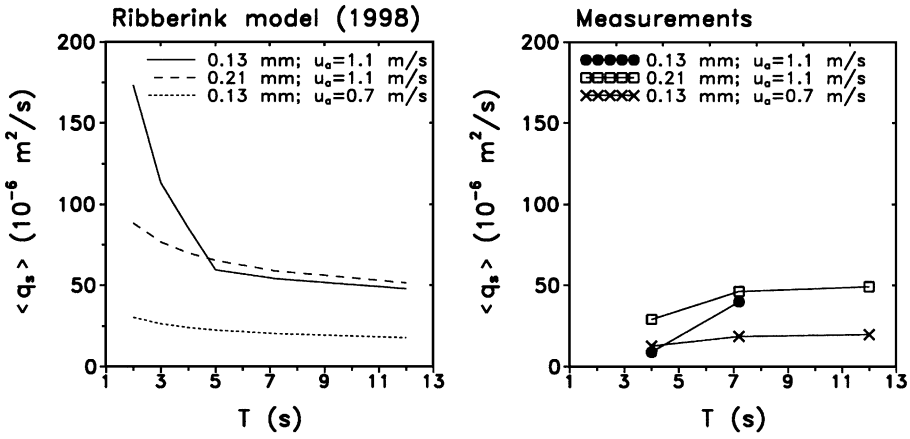

Fig. 10. Net transport rates against wave period for different combinations of oscillatory velocity amplitude and grain size; left-hand-side panel: predictions by the quasi-steady model of Ribberink (1998), right-hand-side panel: measurements.

unsteady model, the occurrence of phase lags would reduce the net transport rates and indeed for almost all these cases measured net transport rates are smaller than predicted by the quasi-steady model.

5. Verification of the new semi-unsteady model

As explained in Section 2, the semi-unsteady model depends on the phase lag parameter, which includes a calibration coefficient α. Based on the present experimental data, we calibrated the semi-unsteady model to determine the value of this coefficient: for each of the test conditions a value of α was determined that was required to fit the measured net transport rates. Averaging the required values of α yielded an optimal value of $\alpha = 0.93$ (standard deviation 0.33). Considering the uncertainties in the model and in the measurements and the variation in the obtained values of α, 0.93 is not sufficiently different from 1 to justify the use of a value of α different than 1. Therefore, results of the semi-unsteady model are presented in which a value of the calibration coefficient $\alpha = 1$ is used.

In the following, it will be investigated whether the semi-unsteady model gives better agreement with the measured data than the quasi-steady model. Thereto, Figs. 11–13 present measured net transport rates and predictions by the quasi-steady model of Ribberink (1998) and the new semi-unsteady model, as a function of oscillatory velocity amplitude (u_a), grain size (D_{50}) and wave period (T). The net current velocity is equal to 0.25 m/s in all figures. The range over which the phase lag parameter p varies is presented in the figures.

The three panels in Fig. 11 show that the quasi-steady model strongly overestimates the net transport rates for fine sand and $u_a > 1.1$ m/s (corresponding to $p > 0.6$). Due to phase lag effects, the semi-unsteady model predicts much smaller net transport rates for these cases, giving a much better agreement with the data. For all other conditions phase lag effects are small ($p \leq 0.6$), the semi-unsteady model predicts almost the same net transport rate as the quasi-steady model and both models agree well with the data.

A similar phenomenon can be observed in Fig. 12, which shows measured and calculated net transport rates against grain size for a high oscillatory velocity ($T = 7.2$ s, $u_a = 1.5$ m/s). The value of the phase lag parameter p is equal to 1.05, 0.19 and 0.12 for the fine, medium and coarse sand, respectively. The figure shows that the quasi-steady model predicts increasing net transport rates for decreasing grain size. For a decrease in grain size from 0.32 to 0.21 mm the measurements show the same trend. However, a further decrease in grain size to 0.13 mm shows a decrease in the measured net transport rate, contrary to the predictions of the quasi-steady model. This decrease in the net transport rate is predicted by the semi-unsteady model, although to a smaller extent

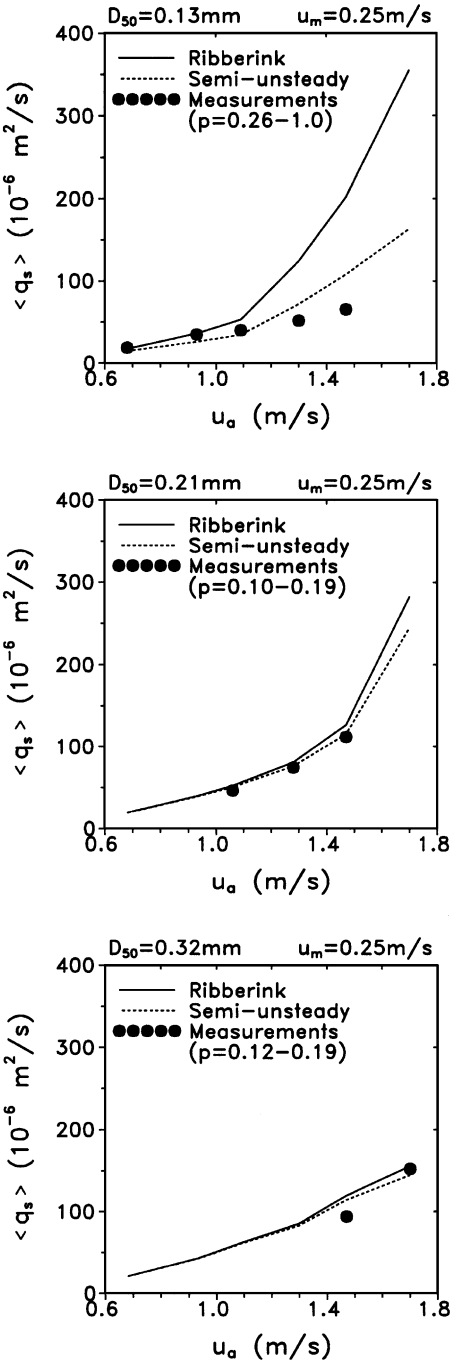

Fig. 11. Measured and calculated net transport rates as a function of oscillatory velocity amplitude u_a for a wave period of 7.2 s and three different grain sizes.

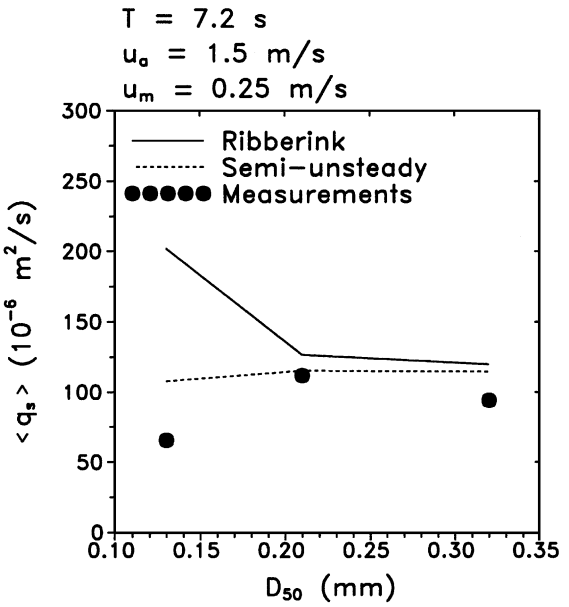

Fig. 12. Measured and calculated net transport rates as a function of grain diameter for one flow condition.

than in the measurements. The large value of the phase lag parameter for the fine sand ($p = 1.05$) leads to a strong reduction of the predicted quasi-steady net transport rate for the fine sand. Therefore, the semi-unsteady model predicts a decrease in net transport rate from medium to fine sand rather than an increase, as predicted by the quasi-steady model.

Finally, Fig. 13 shows measured and calculated net transport rates as a function of wave period. For wave periods $T \geq 7.2$ s (small values of p), both models agree reasonably well with the data. For a decrease in wave period from 7.2 to 4 s the measurements show a decrease in net transport rate, contrary to the predictions of the quasi-steady model. Conditions with a wave period of 4 s correspond to relatively large values of the phase lag parameter p. As a result, the predicted reduction of the quasi-steady transport rate is largest for the smallest wave period. This is in line with the observations, although the reduction in net transport rate is underestimated by the semi-unsteady model.

From the present analysis, it is concluded that even in sheet flow conditions, when sediment particles stay relatively close to the bed, phase lags between the flow velocity and sediment concentration can have a significant effect on the net transport rates. The

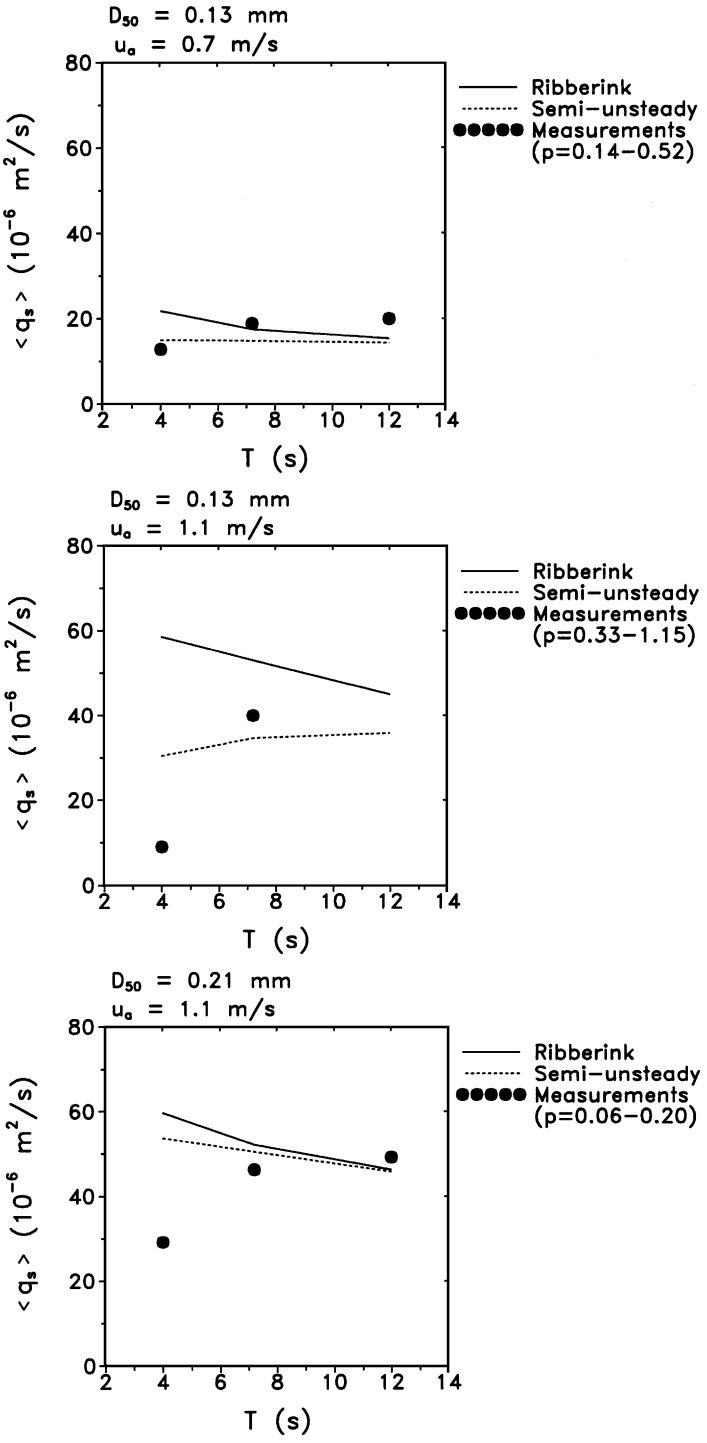

Fig. 13. Measured and calculated net transport rates as a function of wave period.

reduction in the net transport rate due to phase lag effects is described to some extent by the proposed phase lag correction method (semi-unsteady bed load model). The fact that the calibration coefficient α for the phase lag parameter is equal to 1 indicates that phase lags can be characterised by a phase lag parameter p that is equal to $\delta_s\omega/w_s$.

6. Measured time-dependent sediment concentrations

Until now, the occurrence of phase lags is investigated in an indirect way, i.e. by studying the behaviour of the net transport rates. In this section, results of direct time-dependent measurements of sediment concentrations in the sheet flow layer (measured by CCM) are presented, in order to obtain a more direct evidence for the existence of phase lags and to study their character.

Fig. 14 shows measured time-dependent sediment concentrations in the sheet flow layer for three different grain sizes under the same flow condition (H6, E2, I1: $T=7.2$ s, $u_a=1.5$ m/s, $u_m=0.25$ m/s). The upper panels of Fig. 14 present the velocity, measured just outside the wave boundary layer (0.1 m above the bed). Measurements are ensemble-averaged (i.e. averaged at fixed phase) over about 10–20 waves. The level $z=0$ is defined at the initial still bed level. Note that the inaccuracy in bed level measurements is approximately ± 1 mm.

The figure shows that at a certain level below $z=0$ ($z=-3.5$ mm or $z=-4$ mm) the concentration remains almost constant and relatively high ($\approx$ 1000–1400 g/l) throughout the wave cycle. This indicates that no sediment is moving at this level, which can therefore be considered as the top of the non-moving sand bed. The sheet flow layer just above the non-moving sand bed consists of two layers with opposite behaviour.

- The upper sheet flow layer is located above the initial bed level ($z>0$). Here, the concentration increases for increasing velocity because sediment is entrained into the flow. When the velocity decreases the sediment settles down and the concentration decreases again. This process is very similar to an advection–diffusion process that is often observed in the suspension layer.
- The lower layer is called the pick-up layer and is located below the initial bed level ($z<0$). At these low levels the concentration is decreasing for increasing velocities because sediment is being picked up from the bed. When the velocity decreases the sediment settles back toward the bed and the concentration increases again. This behaviour cannot be described by an advection–diffusion approach.

In addition to this general pattern, sharp concentration peaks are observed around flow reversal. The origin of these peaks is not yet fully understood. They may be attributed to shear instabilities in the wave boundary layer (e.g. Foster et al., 1994). In any case, they will be of minor importance to the sediment transport rates, because they have a short duration and occur around the moment of zero velocity. The sediment flux due to these concentration peaks will thus be small and in the following no further attention is paid to these concentration peaks.

The measurements show that the concentrations in the upper sheet flow layer decrease for increasing grain size (compare for example the concentrations around 4–4.5 mm above the still bed level). An important aspect is that the fine sand (phase lag parameter $p=1.05$) reacts slower to changes in the velocity than the two coarser sands ($p<0.2$).

- For the fine sand the increase and decrease in concentration in the upper sheet flow layer occurs much slower than for the two coarser sands and the concentration does not return to zero around flow reversal, as is the case for the two coarser sands. Apparently, not all fine particles settle back to the bed. This seems to be the reason why, for fine sand, the concentration during the negative half wave cycle (when the velocity is lower than during the positive half wave cycle) is almost the same as the concentration during the positive half wave cycle: the concentration asymmetry is much smaller than for the two coarser sands.
- Also for the fine sand the increase and decrease in concentration in the pick-up layer occurs much slower than for the two coarser sands and the concentration does not return to its still bed value around flow reversal, as is the case for the two coarser sands. Again, apparently not all fine particles settle back to the bed.

The very different behaviour of the fine sand is also illustrated in Fig. 15, which shows the ensemble-

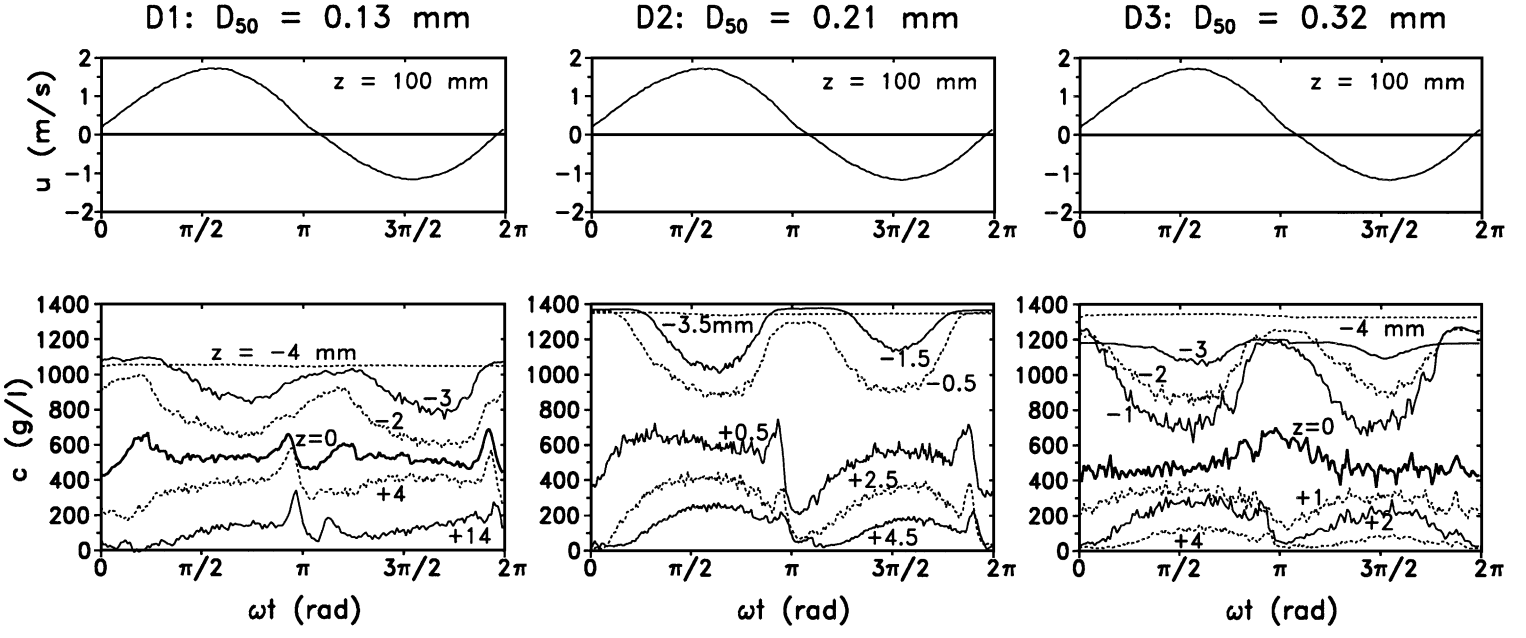

Fig. 14. Measured ensemble-averaged concentrations in the sheet flow layer (lower panels) for three different grain sizes. The upper panels show the velocity at 0.1 m above the bed.

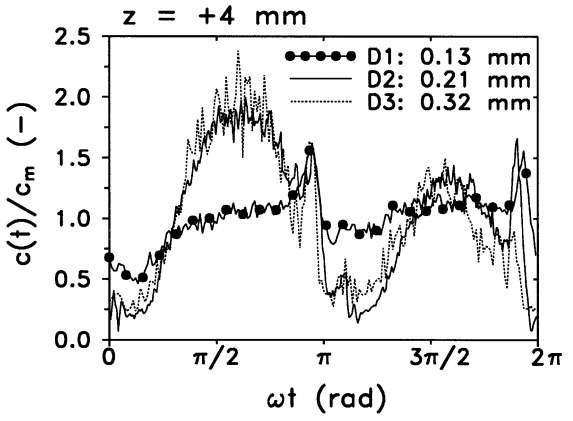

Fig. 15. Non-dimensional concentrations (normalised by the time-averaged values, c_m) at $z=+4$ mm for fine, medium and coarse sand.

averaged concentration at about $z=+4$ mm for the three different sands. Concentrations are normalised by their time-averaged values, c_m. This figure shows clearly that the concentration behaviour of the two coarser sands is similar and very different from the concentration behaviour of the fine sand. For the fine sand both the variation in concentration over time and the concentration asymmetry is much smaller than for the two coarser sands. The smaller concentration asymmetry explains the smaller net transport rates for the fine sand compared to the two coarser sands, despite the much higher concentrations for fine sand.

The measured time-dependent concentrations in the sheet flow layer showed that not all details of the sheet flow could be described by an advection–diffusion approach. This is especially the case for the pick-up layer. However, the measurements do show that even inside the sheet flow layer phase lags occur, despite the small vertical entrainment and settling distances involved (millimetres). Moreover, the measurements confirm the hypothesis that these phase lags increase with increasing values of the phase lag parameter p. Due to these phase lags, differences in sediment concentration between the two (asymmetric) half wave cycles reduce, which results in smaller net transport rates. It can thus be concluded that even in sheet flow conditions phase lags between the flow velocity and the sediment concentration can become so large that they affect (i.e. reduce) the net transport rates.

7. Discussion

7.1. Differences between measurements and the semi-unsteady model

For conditions when the phase lag parameter is large, the measured net transport rates are smaller than predicted by the quasi-steady model of Ribberink (1998). For those cases, the new semi-unsteady model shows much better agreement with the data, although it still gives some overestimation of the net transport rates. This may have several reasons.

- Dohmen-Janssen et al. (2001) found indications that near-bed velocities and concentrations in sheet flow conditions are reduced due to mobile-bed effects (increased roughness and damping of turbulence), caused by the presence of the sheet flow layer. These effects were especially observed for fine sand under high velocities (large sheet flow layer thickness). For these conditions, which correspond to a large phase lag parameter, mobile-bed effects may lead to a additional reductions in net transport rates, which are not caused by phase lags.
- There are some indications that for a short wave period ($T=4$ s), a limited pick-up of sand from the bed may cause an additional reduction in the measured net transport rate. Video recordings of erosion depth showed that several layers of sand grains are eroded from the bed during the wave cycle. For fine sand and a constant flow velocity, erosion depth is smaller for a wave period of 4 s than for a wave period of 7.2 or 12 s (Dohmen-Janssen, 1999), indicating that the amount of sand entrained into the flow (sediment load) is smaller for a wave period of 4 s than for a wave period of 7.2 or 12 s. This is confirmed by measurements of sheet flow layer thickness and sediment concentration, which both are smaller for a wave period of 4 s than for a wave period of 12 s (see Dohmen-Janssen, 1999).

These observations indicate that if the wave period is long compared to the required time to erode the sediment bed, the sediment load will reach its maximum possible value. However, if the wave period is short compared to this "pick-up time", the entrained sediment load may be limited by the available time to erode the sand bed. This may lead to decreasing net transport rates for decreasing wave periods. The maximum possible sediment load can be expected to be large for high flow velocities and fine sediment,

indicating that a limited pick-up may especially occur for large values of the phase lag parameter and thus enlarge phase lag effects.

The phenomenon of limited pick-up is not included in quasi-steady models, which assume an instantaneous sediment response. However, it is neither included in the semi-unsteady model: this model takes into account the delayed settling of the sediment and the time required for particles to travel upward to higher elevations. However, it still assumes an instantaneous pick-up from the bed. Further investigation should reveal whether the phenomenon of limited pick-up does occur and can affect the net transport rates.

7.2. Verification of occurrence of phase lag effects and the semi-unsteady model with other data

Comparison between the present experiments and the proposed semi-unsteady model indicates that phase lag effects can be characterised by the phase lag parameter and that these phase lag effects reduce the net transport rates. However, this analysis is only based on 24 data points. Therefore, the occurrence of phase lags is investigated for other oscillatory sheet flow data sets and the semi-unsteady model is verified against these data sets.

The data used for this verification are obtained from two oscillating water tunnels, i.e. the same large oscillating water tunnel used in the present experiments, and the oscillating water tunnel of the Tokyo University. The data sets cover a range of grain sizes, wave types, wave periods, oscillatory velocities, wave asymmetries (R), and net current velocities, as presented in Table 4. The complete data set consists of 118 sheet flow experiments; 51 from the Delft Hydraulics water tunnel (Ribberink and Al-Salem, 1995; Ribberink and Chen, 1993; Ramadan, 1994; Katopodi et al., 1994 and the present experiments) and 67 from the Tokyo University tunnel (Dibajnia, 1991; Dibajnia and Watanabe, 1992). Because of the short wave periods in the data from the Tokyo University tunnel, this data set includes many experiments that correspond to a large value of the phase lag parameter.

The occurrence of phase lags is investigated by calculating the ratio between the net transport rate predicted by the quasi-steady model of Ribberink (1998) and the measured net transport rate. Fig. 16 shows this ratio, plotted against the phase lag parameter $p = \delta_s\omega/w_s$ for all the experiments in the data set. This figure shows a general trend of an increasing ratio for increasing values of the phase lag parameter p, which confirms the earlier observations that for large values of the phase lag parameter the measured net transport rates are smaller than predicted by the quasi-steady model. This strengthens the conclusion that even in sheet flow conditions phase lags occur (for large values of the phase lag parameter) and that these phase lags lead to a reduction of the net transport rate.

Next, measured net transport rates of the complete data set are compared with predictions of the quasi-steady model of Ribberink (1998) and with predictions of the proposed semi-unsteady model. This is presented in Fig. 17, which shows the calculated net transport rates against the measured values for the quasi-steady model (left hand side panel) and for the semi-unsteady model (right hand side panel). The dashed line represents perfect agreement between the model and the measurements, while the solid lines represent a factor 2 difference. The figure shows clearly that agreement between the data and the predictions is better for the semi-unsteady model than for the quasi-steady model, indicating that predictions are improved if phase lag effects are included. The quasi-steady model of Ribberink especially overpredicts some of the Tokyo data for which the phase lag parameter is high. Almost all overpredictions disappear in the semi-unsteady model and 80–90% of the predictions fall within a factor 2 of the measurements.

Table 4
Data used in verifications

Facility	D_{50} (mm)	Wave type	T (s)	u_{max} (m/s)	R	u_m (m/s)
Tokyo	0.2	cnoidal	2–4	0.6–1.0	0.50–0.80	0–0.20
Delft Hydraulics	0.13–0.32	sine and 2nd-order Stokes	4–12	0.7–2.0	0.55–0.95	0–0.47

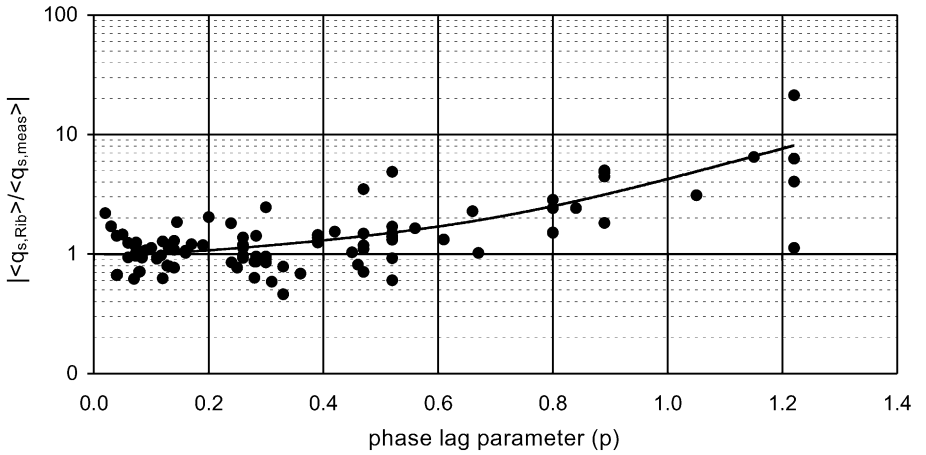

Fig. 16. Ratio of predicted net transport rate (by the quasi-steady model of Ribberink, 1998) and measured net transport rate as a function of the phase lag parameter $p = \delta_s \omega / w_s$.

7.3. Practical relevance of phase lag effects

Measured net transport rates in comparison with the predictions of a quasi-steady and a semi-unsteady model indicate that even in sheet flow conditions net transport rates may be significantly reduced due to phase lags between the velocity and the sediment concentration. This is confirmed by measurements of time-dependent concentrations in the sheet flow layer. According to the proposed phase lag correction method, for wave-dominated sheet flow conditions ($u_m/u_a < 1$), phase lag effects become important if the phase lag parameter p is larger than about 0.5 ($r \leq 0.7$, see Fig. 1):

$$p = \frac{\delta_s \omega}{w_s} > 0.5 \tag{17}$$

Because Dohmen-Janssen et al. (2001) found that the sheet flow layer thickness δ_s is larger for fine sand ($D_{50} = 0.13$ mm) than for coarser sand ($D_{50} \geq 0.21$

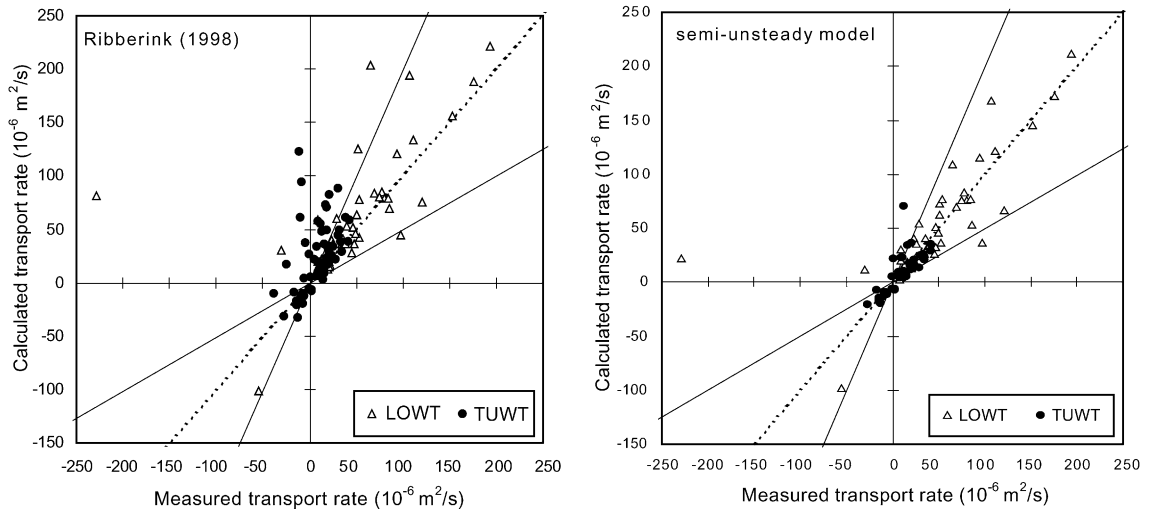

Fig. 17. Predicted against measured net transport rates; quasi-steady model of Ribberink (1998) (left-hand-side panel) and the proposed semi-unsteady model (right-hand-side panel).

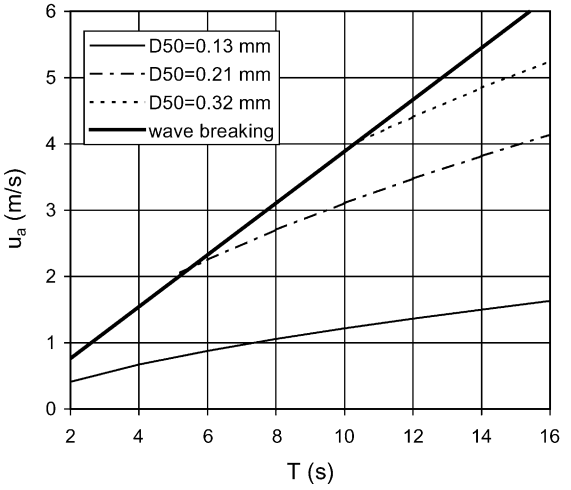

Fig. 18. Oscillatory velocity amplitude u_a against wave period T. Dividing lines between unsteady and quasi-steady behaviour ($p=0.5$) for three grain sizes.

mm), phase lag effects are especially important for fine sand: for fine sand the fall velocity w_s is small, but at the same time δ_s is large. By substituting the expressions for the sheet flow layer thickness δ_s (Eq. (2)) in Eq. (17), criteria for the occurrence of phase lag effects can be worked out in terms of known parameters (D_{50}, w_s, ω and the Shields parameter θ_w):

$$\frac{\theta_w D_{50}\omega}{w_s} > 0.014 \qquad \text{for} D_{50} = 0.13\text{mm}$$

$$\frac{\theta_w D_{50}\omega}{w_s} > 0.038 \qquad \text{for } D_{50} \geq 0.21 \text{ mm} \tag{18}$$

Assuming a certain friction factor f_w this can be expressed in terms of grain size, oscillatory velocity amplitude and wave period. Fig. 18 shows for three grain sizes combinations of oscillatory velocity amplitudes u_a and wave periods T that lead to a value of $p=0.5$. For each sand size, phase lag effects can be expected for combinations of u_a and T that are located above the lines. In order to show which conditions are realistic and can be expected in the field, the figure also includes the wave breaking criterion of Miche (1951): $H_{br}=\gamma h$, with H_{br} the wave height at breaking, h the water depth and γ the breaker coefficient which is assumed to be 0.5. Applying linear wave theory and shallow water approximations yields a limiting combination of u_a and T for which waves will break:

$$u_a = \frac{\omega \frac{1}{2} H_{br}}{kh} = \frac{1}{2}\gamma\frac{\omega}{k} = \frac{1}{2}\gamma\frac{gT}{2\pi} \tag{19}$$

Here k is the wave number ($k=2\pi/L$, with L the wave length) and g is the gravity acceleration. This means that waves break if $u_a/T > \gamma g/4\pi = 0.39$. The figure shows indeed that for fine sand, phase lag effects can become important in a wide range of wave conditions. For coarser sands ($D_{50} \geq 0.21$ mm), the transport will generally behave in a quasi-steady way, except for extremely high velocities ($u_a > 2.5$ m/s).

The present analysis is based on an oscillatory flow that consists of a sinusoidal oscillatory component and a net current. However, waves in shallow water are not sinusoidal, but have a more asymmetric shape (high crests, shallow troughs). In case of a second-order Stokes wave without a net current, the near-bed velocity is given by: $u_\infty(t) = u_1\cos(\omega t) + u_2 \cos(2\omega t)$. Appendix B shows that in that case the phase lag correction factor r is given by:

$$r = \frac{2}{3}F_1(p) + \frac{1}{3}F_2(p) \tag{20}$$

Here $F_1(p)$ and $F_2(p)$ are analytical functions of the parameter p that can be found in Appendix B.

For the situations of a sinusoidal oscillatory flow and a second-order Stokes oscillatory flow, both without a net current, the relation between p and r is presented in Fig. 19. This figure shows that phase lags

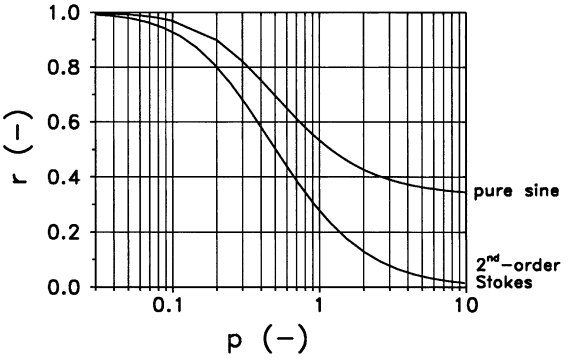

Fig. 19. Calculated values of phase lag correction factor r as a function of phase lag parameter p for sinusoidal oscillatory flow and for second-order Stokes oscillatory flow.

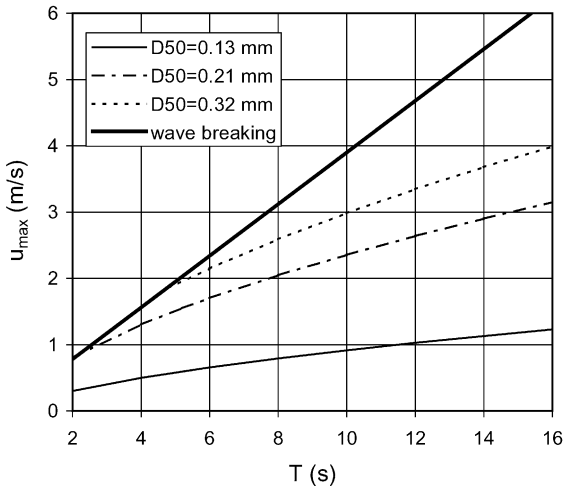

Fig. 20. Maximum velocity u_{max} for second-order Stokes oscillatory flow against wave period T. Dividing lines between unsteady and quasi-steady behaviour ($p=0.3$) for three grain sizes.

in asymmetric waves lead to stronger reductions of the net transport rates: $r \leq 0.7$ for $p \geq 0.3$. Based on this result, Fig. 20 shows for three grain sizes combinations of maximum second-order Stokes oscillatory velocities ($u_{max}=u_1+u_2$) and wave periods that lead to a value of $p=0.3$. Because this analysis is only meant as a first indication of the practical relevance of phase lag effects the wave breaking criterion is estimated as $u_{max}/T>0.39$. This figure shows that phase lag effects will often occur for fine sand and become important for coarser sands in the high velocity regime.

8. Conclusions

The present study shows that even in sheet flow conditions phase lags between sediment concentrations and near-bed oscillatory velocities can become so large that *net* transport rates are reduced. This is the case if the phase lag parameter $p=\delta_s\omega/w_s$ becomes larger than about 0.5. The parameter p is proportional to the fall time of a sediment particle (entrained to a height that is equal to the thickness of the sheet flow layer δ_s) and the wave period. For small phase lags ($p<0.5$) net transport rates, measured in a large oscillating water tunnel, are predicted well by the quasi-steady model of Ribberink (1998). If phase lags become significant ($p>0.5$) measured net transport rates are smaller than predicted by this quasi-steady model. In that case, the proposed semi-unsteady model that predicts phase lag effects based on the value of the parameter p gives better agreement with the data. The occurrence of phase lags is confirmed by a larger data set that shows that for high values of the phase lag parameter, net transport rates are overestimated by the quasi-steady model. Also for these data, the proposed semi-unsteady model yields better agreement with the data than the quasi-steady model.

The occurrence of phase lags inside the sheet flow layer is also confirmed by time-dependent concentration measurements, which show that for large values of the phase lag parameter p, concentrations lag significantly behind the velocity, even inside the sheet flow layer. This leads to a smaller concentration asymmetry between the two half cycles, which reduces the *net* transport rate.

Especially for fine sand (D_{50} around 0.13 mm), conditions that lead to phase lag effects are common in the field. For coarser sand (D_{50} around 0.2 mm) phase lags may still be common, but only under high oscillatory velocities ($u>1.5$ m/s).

Acknowledgements

The project was funded by the Technology Foundation (STW), project DCT.2912. The authors wish to thank the Dutch Ministry of Transport and Public Works (RIKZ) for the financial support to perform the experiments. The help of Remmelt van der Wal and Ella van der Hout in performing the experiments and analysing part of the data is greatly acknowledged. Finally, we would like to thank Mohammad Dibajnia for providing his sheet flow data.

Appendix A. Calculation of combined wave–current friction factor

In the present study, the wave–current friction factor f_{cw} is calculated according to the expression of Madsen and Grant (1976):

$$f_{cw}=f_c+(1-\alpha)f_w, \qquad \text{with } \alpha=\frac{u_m}{u_a+u_m} \qquad (I.1)$$

Here, u_m is the time-averaged horizontal velocity at a near-bed level z_{um}, outside the wave boundary layer and u_a is the amplitude of the free-stream oscillatory velocity. The wave friction factor f_w is calculated according to the formula of Swart (1974), which is an explicit approximation to the implicit formula given by Jonsson (1966). The expression reads:

$$f_w = \exp\left[-5.997 + 5.213\left(\frac{k_s}{a}\right)^{0.194}\right] \tag{I.2}$$

Here k_s is the equivalent Nikuradse bed roughness height and a is the semi-excursion length of the orbital motion ($a = u_a/\omega = u_a T/2\pi$, with ω the angular frequency of the wave and T the wave period). The current friction factor f_c is derived by assuming a logarithmic velocity distribution with height in the near-bed layer:

$$f_c = 2\kappa^2\left[\ln\left(\frac{z_{um}}{z_0}\right)\right]^{-2} \tag{I.3}$$

Here, κ is the von Kármán constant, which is equal to 0.4, z_0 is the level where the velocity is assumed to be zero ($z_0 = k_s/30$) and z_{um} is the level where the velocity u_m is specified.

Appendix B. Derivation of phase lag correction factor *r*

For practical reasons, the free-stream velocity $u_\infty(t)$ is here rewritten as:

$$u_\infty(t) = \sum_{k=0}^{N} u_k \cos(k\omega t) \tag{II.1}$$

In the present derivation, a time-averaged component u_0 ($= u_m$), a first harmonic component u_1 ($= u_a$) and a second harmonic component u_2 are considered, i.e. $N = 2$. However, the derivation can be extended to larger values of N.

In order to solve the advection–diffusion equation for the real concentration (Eq. (9)) and for the quasi-steady concentration (Eq. (9) with $\partial c/\partial t = 0$), two boundary conditions are required for each situation. Both the quasi-steady and the real concentrations are assumed to be zero at the upper boundary ($c_r = c_{qs} = 0$ at $z = z_\infty$). At the bottom ($z = 0$) it is assumed that the real sediment concentration gradient is the same as in the quasi steady condition:

$$\left.\frac{\partial c_r}{\partial z}\right|_{z=0} = \left.\frac{\partial c_{qs}}{\partial z}\right|_{z=0} = -\frac{w_s c_{qs}(0,t)}{\varepsilon_s} \tag{II.2}$$

The quasi steady bottom concentration $c_{qs}(0,t)$ is assumed to be a power function of the velocity $u_\infty(t)$:

$$c_{qs}(0,t) = a\,|\,u_\infty(t)^b\,| \tag{II.3}$$

The advection–diffusion Eq. (9) has analytical solutions only if the exponent b in the expression for the bottom boundary condition is even. Because the sand transport rate is equal to the product of velocity and concentration, the sand transport rate is proportional to the velocity to the power $b+1$. For large velocities, the transport rate in the bed load model of Ribberink (1998) is roughly proportional to $u^{3.3}$. Therefore, here $b = 2$ is chosen, giving a transport rate proportional to u^3. Applying these considerations results in the following expressions for the real and the quasi steady sediment concentration:

$$c_r(z,t) = \sum_{k=0}^{2b}\left[\frac{\hat{c}_{bot,k}}{\sqrt{(P_k^2 + Q_k^2)}}\exp\left(-\frac{w_s z}{\varepsilon_s}P_k\right) \times \cos\left(k\omega t - \frac{w_s z}{\varepsilon_s}Q_k + \varphi_k\right)\right] \tag{II.4}$$

$$c_{qs}(z,t) = \sum_{k=0}^{2b}\left[\hat{c}_{bot,k}\exp\left(-\frac{w_s z}{\varepsilon_s}\right)\cos(k\omega t)\right] \tag{II.5}$$

With:

$$\hat{c}_{bot,0} = a\left(u_0^2 + \frac{1}{2}u_1^2 + \frac{1}{2}u_2^2\right) \tag{II.6}$$

$$\hat{c}_{bot,1} = a(2u_0u_1 + u_1u_2) \tag{II.7}$$

$$\hat{c}_{bot,2} = a\left(2u_0u_2 + \frac{1}{2}u_1^2\right) \tag{II.8}$$

$$\hat{c}_{bot,3} = a(u_1u_2) \tag{II.9}$$

$$\hat{c}_{\mathrm{bot},4} = a\left(\frac{1}{2}u_1^2\right) \tag{II.10}$$

$$P_k = \frac{1}{2} + \left[\frac{1}{16} + (kp)^2\right]^{1/4} \cos\left(\frac{1}{2}\alpha_k\right) \tag{II.11}$$

$$Q_k = \left[\frac{1}{16} + (kp)^2\right]^{1/4} \sin\left(\frac{1}{2}\alpha_k\right) \tag{II.12}$$

$$\alpha_k = \arctan(4kp) \tag{II.13}$$

$$\varphi_k = \arctan\left(-\frac{Q_k}{P_k}\right) \tag{II.14}$$

$$p = \frac{\varepsilon_s \omega}{w_s^2} \tag{II.15}$$

Because the expressions are used to calculate the *ratio* of the real and quasi steady transport rate, the coefficient a in the expressions for the bottom concentration (Eqs. (II.6), (II.7) and (II.8)) does not need to be known. The equations show that the real concentration $c_r(z,t)$ becomes equal to the quasi-steady concentration $c_{qs}(z,t)$ if the phase lag parameter p is zero. The real and quasi-steady sand transport rates can be derived by multiplying the velocity $u_\infty(t)$ with the vertical integral of the sediment concentration. The real and quasi steady transport rate are given by:

$$q_{s,r}(t) = \left[\sum_{k=0}^{N} u_k \cos(k\omega t)\right]\left[\sum_{k=0}^{2b}\left(\frac{\varepsilon_s}{w_s}\frac{\hat{c}_{\mathrm{bot},k}}{(P_k^2+Q_k^2)^{3/2}} \times \left[P_k\cos(k\omega t+\varphi_k) + Q_k \sin(k\omega t+\varphi_k)\right]\right)\right] \tag{II.16}$$

$$q_{s,qs}(t) = \left[\sum_{k=0}^{N} u_k \cos(k\omega t)\right] \times \left[\sum_{k=0}^{2b}\left(\frac{\varepsilon_s}{w_s}\hat{c}_{\mathrm{bot},k}\cos(k\omega t)\right)\right] \tag{II.17}$$

The correction factor r is defined as the ratio of the *net* real sand transport rate to the *net* quasi-steady sand transport rate. These net sand transport rates can be determined by averaging Eqs. (II.16) and (II.17) over time. Components of the concentration with an order higher than N (highest order in the velocity) do not contribute to the *net* transport rate. Therefore, the net transport rates are given by:

$$\langle q_{s,r}\rangle = \frac{\varepsilon_s}{w_s}u_0\hat{c}_{\mathrm{bot},0} + \frac{1}{2}\frac{\varepsilon_s}{w_s}\sum_{k=1}^{N}\left(u_k\hat{c}_{\mathrm{bot},k}\frac{P_k}{P_k^2+Q_k^2}\right) \tag{II.18}$$

$$\langle q_{s,qs}\rangle = \frac{\varepsilon_s}{w_s}u_0\hat{c}_{\mathrm{bot},0} + \frac{1}{2}\frac{\varepsilon_s}{w_s}\sum_{k=1}^{N}\left(u_k\hat{c}_{\mathrm{bot},k}\right) \tag{II.19}$$

The phase lag correction factor r then becomes:

$$r = \frac{\langle q_{s,r}\rangle}{\langle q_{s,qs}\rangle} = \frac{u_0\hat{c}_{\mathrm{bot},0} + \frac{1}{2}u_1\hat{c}_{\mathrm{bot},1}F_1(p) + \frac{1}{2}u_2\hat{c}_{\mathrm{bot},2}F_2(p)}{u_0\hat{c}_{\mathrm{bot},0} + \frac{1}{2}u_1\hat{c}_{\mathrm{bot},1} + \frac{1}{2}u_2\hat{c}_{\mathrm{bot},2}} \tag{II.20}$$

with:

$$F_k(p) = \frac{P_k\cos\varphi_k + Q_k\sin\varphi_k}{(P_k^2+Q_k^2)^{3/2}} \tag{II.21}$$

Substituting the expressions for $\hat{c}_{\mathrm{bot},k}$ (i.e. Eqs. (II.6)–(II.8)) yields the following expression for the reduction coefficient r:

$$r = \frac{u_0^3 + \frac{1}{2}u_0u_1^2 + \frac{1}{2}u_0u_2^2 + u_0u_1^2F_1(p) + \frac{1}{2}u_1^2u_2F_1(p) + u_0u_2^2F_2(p) + \frac{1}{4}u_1^2u_2F_2(p)}{u_0^3 + \frac{3}{2}u_0u_1^2 + \frac{3}{2}u_0u_2^2 + \frac{3}{4}u_1^2u_2} \tag{II.22}$$

In case of a sinusoidal oscillatory flow with a net current (i.e. $u_2 = 0$) this reduces to:

$$r = \frac{\left(\frac{u_0}{u_1}\right)^2 + \frac{1}{2} + F_1(p)}{\left(\frac{u_0}{u_1}\right)^2 + \frac{3}{2}} \qquad \text{(II.23)}$$

In case of a second-order oscillatory flow without a net current (i.e. $u_0 = 0$), this reduces to:

$$r = \frac{2}{3}F_1(p) + \frac{1}{3}F_2(p) \qquad \text{(II.24)}$$

Appendix C. Main notation

a	semi-excursion length of orbital motion ($=u/\omega$), m
c	sediment concentration, g/l, kg/m^3 or m^3/m^3
c_m	time-averaged concentration, g/l or kg/m^3
D_{50}	median grain size, m
f_c	current friction factor, non-dimensional
f_w	wave friction factor, non-dimensional
f_{cw}	combined wave–current friction factor, non-dimensional
g	gravity acceleration, m/s^2
k_s	bed roughness height, m
p	phase lag parameter (Eqs. (12) and (13)), non-dimensional
q_s	sand transport rate, m^3/s/m
$\langle q_s \rangle$	net (i.e. wave-averaged) sand transport rate, m^3/s/m
r	phase lag correction factor (Eq. (11)), non-dimensional
s	relative density $= \rho_s/\rho$, non-dimensional
t	time, s
t_{fall}	fall time of a sediment particle $= \delta/w_s$, s
T	wave period, s
u	horizontal near-bed velocity, m/s
u_a	amplitude of horizontal oscillatory velocity, m/s
u_m	time-averaged horizontal velocity, m/s
w_s	settling velocity of a single sediment particle, m/s
x	distance in flow (u) direction, m
z	level above the bed, m
δ	height to which a particle is entrained into the flow, m
δ_s	sheet flow layer thickness, m
ε_s	vertical sediment diffusivity, m^2/s
θ	Shields parameter, non-dimensional
θ_{cr}	critical Shields parameter, non-dimensional
θ_w	maximum Shields parameter in oscillatory flow (based on u_a), non-dimensional
θ_{cw}	maximum Shields parameter in combined wave–current flow (based on $u_{max} = u_a + u_m$), non-dimensional
ρ	density of water, kg/m^3
ρ_s	density of the sediment, kg/m^3
τ_b	bed shear stress, N/m^2
ω	angular frequency of the wave ($=2\pi/T$), rad/s

References

Asano, T., 1992. Observations of granular–fluid mixture under an oscillatory sheet flow. Proc. 23rd Int. Conf. on Coast. Eng., New York, pp. 1896–1909.

Bailard, J.A., 1981. An energetics total load sediment transport model for a plane sloping beach. J. Geophys. Res. 86 (C11), 10938–10954.

Davies, A.G., Ribberink, J.S., Temperville, A., Zyserman, J.A., 1997. Comparisons between sediment transport models and observations made in wave and current flows above plane beds. Coastal Eng. 31, 163–198.

Dibajnia, M., 1991. Study on Nonlinear effects in beach processes. PhD Thesis, University of Tokyo, September 1991, 105 pp.

Dibajnia, M., Watanabe, A., 1992. Sheet flow under nonlinear waves and currents. Proc. of the 23rd Int. Conf. on Coastal Eng., Venice, pp. 2015–2028.

Dohmen-Janssen, C.M., 1999. Grain size influence on sediment transport in oscillatory sheet flow. Phase-lags and mobile-bed effects. PhD Thesis, Delft Univ. of Techn., The Netherlands, ISBN 90-9012929-4.

Dohmen-Janssen, C.M., Hassan, W.N., Ribberink, J.S., 2001. Mobile-bed effects in oscillatory sheet flow. J. Geophys. Res. 106 (C11), 27103–27115.

Foster, D.L., Holman, R.A., Beach, R.A., 1994. Sediment suspension events and shear instabilities in the bottom boundary layer. Proc. Coastal Dynamics '94, ASCE, Spain, Feb. 1994, pp. 712–726.

Guy, H.P., Simons, D.B., Richardson, E.V., 1966. Summary of alluvial channel data from flume experiments, 1956–1961. U.S. Geol. Surv. Prof. Pap. 462-I Washington, DC.

Horikawa, H., Watanabe, A., Katori, S., 1982. Sediment transport under sheet flow condition. Proc. 18th Int. Conf. on Coastal Eng., Cape Town, pp. 1335–1352.

Inman, D.L., Jenkins, S.A., Hicks, D.M., Kim, H.K., 1986. Oscillatory bursting over beds of Fine Sand. Ref. Series 86-13, Scripps Inst. of Oceanography, Univ. of California, San Diego, 16 pp.

Janssen, C.M., 1995. Sand transport in oscillatory sheet-flow; a

literature review. Com. on Hydr. and Geot. Eng., Rep. no. 95-6, issn 0169-6548, Delft Univ. of Tech., The Netherlands.

Jonsson, I.G., 1966. Wave boundary layers and friction factors. Proc. 10th Int. Conf. on Coastal Eng., pp. 27–148.

Katopodi, I., Ribberink, J.S., Ruol, P., Lodahl, C., 1994. Sediment transport measurements in combined wave–current flows. Proc. Coastal Dynamics '94, ASCE, Barcelona, Spain, Feb. 1994.

King, D.B., 1991. Studies in oscillatory flow bedload sediment transport. PhD Thesis, University of California, San Diego.

Klopman, G., 1994. Vertical structure of the flow due to waves and currents. Report H840.30, Part II, Delft Hydraulics, The Netherlands.

Li, L., Sawamoto, M., 1995. Experiments on sediment transport in sheet-flow regime under oscillatory flow. Coastal Eng. Jpn. 38 (2), 143–156.

Madsen, O.S., Grant, W.D., 1976. Sediment transport in the coastal environment. Rep. 209, Ralph M. Parsons Lab. for Water Resources and Hydrodynamics, M.I.T., Cambridge, MA.

Miche, R., 1951. Le pouvoir réfléchissant des ouvrages maritimes exposés à l'action de la houle. Ann. Ponts Chaussees 121, 285–319.

Nielsen, P., 1979. Some basic concepts of wave sediment transport. Inst. of Hydrodyn. and Hydr. Eng., Tech. Univ. of Denmark, series Paper no. 20.

Nnadi, F.N., Wilson, K.C., 1992. Motion of contact-load particles at high shear stress. J. Hydraul. Eng. 118 (12), 1–15.

Ramadan, K.A.H., 1994. Time-averaged sediment transport phenomena in combined wave–current flows. Report H1889.11, Part I, January 1994, Delft Hydraulics, The Netherlands.

Ribberink, J.S., 1998. Bed-load transport for steady flows and unsteady oscillatory flows. Coastal Eng. 34, 59–82.

Ribberink, J.S., Al-Salem, A.A., 1992. Sediment transport, sediment concentrations and bedforms in simulated asymmetric wave conditions—experimental study in the large oscillating water tunnel of Delft Hydraulics. Data Report H840.20, Part V, April 1992, Delft Hydraulics, The Netherlands.

Ribberink, J.S., Al-Salem, A.A., 1994. Sediment transport in oscillatory boundary layers in cases of rippled bed and sheet-flow. J. Geophys. Res. 99 (C6), 12707–12727.

Ribberink, J.S., Al-Salem, A.A., 1995. Sheet flow and suspension in oscillatory boundary layers. Coastal Eng. 25, 205–225.

Ribberink, J.S., Chen, Z., 1993. Sediment transport of fine sand under asymmetric oscillatory flow. Report H840, Part VII, January 1993, Delft Hydraulics, The Netherlands.

Ribberink, J.S., Katopodi, I., Ramadan, K.A.H., Koelewijn, R., Longo, S., 1994. Sediment transport under (non)linear waves and currents. Proc. 24th Int. Conf. on Coastal Eng., Japan, 2527–2541.

Richardson, Y.F., Zaki, W.N., 1954. Sedimentation and Fluidization. Part I. Trans. Inst. Chem. Eng. 32, 35–53.

Sawamoto, M., Yamashita, T., 1986. Sediment transport rate due to wave action. J. Hydrosc. Hydraul. Eng. 4 (1), 1–15.

Sleath, J.F.A., 1994. Sediment transport in oscillatory flow. In: Belorgey, M., Rajaona, R.D., Sleath, J.F.A. (Eds.), Sediment Transport Mechanisms in Coastal Environments and Rivers. World Scientific, River Edge, NJ, pp. 93–106.

Sleath, J.F.A., 1999. Conditions for plug formation in oscillatory flow. Cont. Shelf Res. 19, 1643–1664.

Swart, D.H., 1974. Offshore sediment transport and equilibrium beach profiles. Delft Hydr. Lab. Publ., No. 131, Delft Hydraulics, The Netherlands.

Sumer, B.M., Kozakiewicz, A., Fredsoe, J., Deigaard, R., 1996. Velocity and concentration profiles in sheet-flow layer of movable bed. J. Hydraul. Eng., ASCE 122 (10), 549–558.

Van den Berg, J.H., 1986. Aspects of sediment and morphodynamics of subtidal deposits of the Oosterschelde (The Netherlands), Rijkswaterstaat Communications No. 43.

Wilson, K.C., 1987. Analysis of bed-load motion at high shear stress. J. Hydraul. Eng., ASCE 113 (1), 97–103.

Zala Flores, N., Sleath, J.F.A., 1998. Mobile layer in oscillatory sheet flow. J. Geophys. Res. 103 (C6), 12783–12793.